Available online at www.sciencedirect.com

ScienceDirect

Geochimica et Cosmochimica Acta 177 (2016) 254–274

Geochimica et Cosmochimica Acta

www.elsevier.com/locate/gca

Chemical evidence for differentiation, evaporation and recondensation from silicate clasts in Gujba

Jonathan Oulton [a], Munir Humayun [a,*], Alexei Fedkin [b], Lawrence Grossman [b,c]

[a] National High Magnetic Field Laboratory & Department of Earth, Ocean and Atmospheric Science, Florida State University, Tallahassee, FL 32310, USA

[b] Department of the Geophysical Sciences, The University of Chicago, Chicago, IL 60637, USA

[c] Enrico Fermi Institute, The University of Chicago, Chicago, IL 60637, USA

Received 21 June 2015; accepted in revised form 14 January 2016; Available online 23 January 2016

Abstract

The silicate and metal clasts in CB chondrites have been inferred to form as condensates from an impact-generated vapor plume between a metal-rich body and a silicate body. A detailed study of the condensation of impact-generated vapor plumes showed that the range of CB silicate clast compositions could not be successfully explained without invoking a chemically differentiated target. Here, we report the most comprehensive elemental study yet performed on CB silicates with 32 silicate clasts from nine slices of Gujba analyzed by laser ablation inductively coupled plasma mass spectrometry for 53 elements. Like in other studies of CBs, the silicate clasts are either barred olivine (BO) or cryptocrystalline (CC) in texture. In major elements, the Gujba silicate clasts ranged from chondritic to refractory enriched. Refractory element abundances ranged from 2 to 10 × CI, with notable anomalies in Ba, Ce, Eu, and U abundances. The two most refractory-enriched BO clasts exhibited negative Ce anomalies and were depleted in U relative to Th, characteristic of volatilization residues, while other BO clasts and the CC clasts exhibited positive Ce anomalies with excess U (1–3 × CI), and Ba (1–6 × CI) anomalies indicating recondensation of ultra-refractory element depleted vapor. The Rare Earth Elements (REE) also exhibit light REE (LREE) enrichment or depletion in several clasts with a range of $(La/Sm)_{CI}$ of 0.9–1.8. This variation in the LREE is essentially impossible to accomplish by processes involving vapor–liquid or vapor–solid exchange of REE, and appears to have been inherited from a differentiated target. The most distinctive evidence for inherited chemical differentiation is observed in highly refractory element (Sc, Zr, Nb, Hf, Ta, Th) systematics. The Gujba clasts exhibit fractionations in Nb/Ta that correlate positively with Zr/Hf and span the range known from lunar and Martian basalts, and exceed the range in Zr/Hf variation known from eucrites. Variations of highly incompatible refractory elements (e.g., Th) against less incompatible elements (e.g., Zr, Sr, Sc) are not chondritic, but exhibit distinctly higher Th abundances requiring a differentiated crust to be admixed with depleted mantle in ratios that are biased to higher crust/mantle ratios than in a chondritic body. The possibility that these variations are due to admixture of refractory inclusion-debris into normal chondritic matter is raised but cannot be definitively tested because existing "bulk" analyses of CAIs carry artifacts of unrepresentative sampling. The inferences drawn from the compositions of Gujba silicate clasts, here, complement what has been inferred from the compositions of metallic clasts, but provide surprisingly detailed insight into the structure of the target. Evidence that metal and silicate in CB chondrites both formed from impact-generated vapor plumes, taken together with recent work on metallic nodules in E chondrites, and on ordinary chondrites, indicates that chondrule formation occurs by this mechanism quite widely. However, the nature of

* Corresponding author.

E-mail addresses: jjo11d@my.fsu.edu (J. Oulton), humayun@magnet.fsu.edu (M. Humayun), avf@uchicago.edu (A. Fedkin), yosi@uchicago.edu (L. Grossman).

http://dx.doi.org/10.1016/j.gca.2016.01.008

the impact on the CB body is quite different than the popular conceptions of impact of partially or wholly molten chondritic bodies and the younger (5 Ma) age of CB chondrules is consistent with origin in a disk with more evolved targets and impactors gravitationally perturbed by nascent planets.

1. INTRODUCTION

The heat source for the origin of chondrules has proven elusive (Zanda, 2004), but might include nebular shocks (Desch and Connolly, 2002; Morris and Desch, 2010) or protoplanetary impacts of partially differentiated bodies (Zook, 1981; Sanders, 1996; Chen et al., 1998; Lugmair and Shukolyukov, 2001; Krot et al., 2005; Hevey and Sanders, 2006; Asphaug et al., 2011), or even a hybrid model (Ruzicka, 2012). An impact origin of chondrules is receiving increasing attention (Asphaug et al., 2011; Sanders and Scott, 2012). Chronologic constraints indicate that chondrules may have formed ~2 Ma after CAIs (e.g., Amelin et al., 2002), contemporaneously with or later than the earliest differentiated bodies (Kleine et al., 2009). Paleomagnetic observations on chondrites (Carpozen et al., 2011) have led to models of partially differentiated chondrite parent bodies (Elkins-Tanton et al., 2011) that, on impact disruption, could lead to the release of abundant molten droplets (Asphaug et al., 2011). Meteoritic constraints implying an impact origin for chondrules include the Fa-content of ordinary chondrite chondrules (Fedkin et al., 2012), sodium retention during chondrule melting (Fedkin and Grossman, 2013) and differentiated siderophile element patterns in metal-sulfide-silicate assemblages in enstatite chondrites (van Niekirk et al., 2009; Horstmann et al., 2014). Among the carbonaceous chondrites, the CB chondrites have attracted the most attention as potential products of protoplanetary impacts (Kallemeyn et al., 1978; Wasson and Kallemeyn, 1990; Krot et al., 2001b, 2005; Campbell et al., 2002, 2005; Rubin et al., 2003; Fedkin et al., 2015).

CB chondrites are a group of metal-rich carbonaceous chondrites (Krot et al., 2002) that are characterized petrographically by rounded barred olivine (BO) and cryptocrystalline (CC) silicate clasts, abundant Fe–Ni metal spheroids, and a dark silicate matrix containing both brecciated clast material and veins of shock-impact melt (Weisberg and Kimura, 2010). Elemental studies have shown that CBs are severely depleted in volatile elements and enriched in refractory elements (Kallemeyn et al., 1978; Krot et al., 2001a; Campbell et al., 2002; Rubin et al., 2003). CBs contain isotopically heavy nitrogen (Prombo and Clayton, 1985; Franchi et al., 1986; Sugiura et al., 2000), which together with oxygen isotopic studies have revealed a potential genetic link between CBs and CR/CH chondrites (Weisberg et al., 1990; Krot et al., 2002). The CB chondrites are further classified into two subgroups (Weisberg et al., 2001). Meteorites of the CB_a subgroup include Bencubbin, Gujba, Weatherford, etc., which contain ~40 vol% silicate clasts, ~50 vol% metal, and ~10 vol% matrix, and clast size ranges from millimeters to centimeters. Silicate clasts are FeO-poor, metals contain 5–8 wt% Ni, and the bulk chondrites exhibit $\delta^{15}N$ up to +1000 ‰. Meteorites of the CB_b subgroup include QUE94411, Hammadah al Hamra (HaH) 237, etc., which contain ~30 vol% silicate clasts, ~70 vol% metal, and <5 vol% matrix, and clast sizes are constrained to millimeter-scale. Metals contain 4–15 wt% Ni, and bulk $\delta^{15}N$ is up to +200 ‰ (Weisberg et al., 2001). Additionally, CB_b metal grains containing >7–8 wt% Ni are chemically zoned in Ni, Co and refractory PGEs (decreasing core-rim), and Cr (increasing core-rim) (Meibom et al., 2000; Campbell et al., 2001, 2002, 2005).

Siderophile element studies of the large metal clasts in Gujba and other CB_a's showed that Pd behaved more like a refractory element (e.g., Ir) than like Fe, which occurs only at high temperatures and at pressures well above canonical nebular conditions requiring condensation of the metal from an impact-induced vapor plume (Campbell et al., 2002; Fedkin et al., 2015). Other evidence, including the chondritic Ni-Co systematics of the metal, has been cited that supports that CBs or some of their components originated by condensation from the solar nebula (Newsom and Drake, 1979; Weisberg et al., 1990, 2001). The relationship between the metal and silicate clasts is unclear since the silicate clasts have virtually no metal and there are no isotopic clues that have been able to link the two types of clasts in CBs. Krot et al. (2001a) described the major element and rare earth element (REE) abundances in silicate clasts from CB_b chondrites. They reported two types of chondrules: those with barred olivine (BO) texture were enriched in Ca, Al and REE, and those with cryptocrystalline (CC) texture were chondritic to depleted in Ca, Al and REE. These distinct chemical and textural relations were interpreted to originate by fractional condensation from an impact plume (Krot et al., 2001b, 2005).

Fedkin et al. (2015) developed a model for condensation from an impact plume following Campbell et al. (2002) and Krot et al. (2001b, 2005) that explained the available constraints on metal and on silicate clasts in CBs. Their study found that the composition of the silicate clasts reported by Krot et al. (2001a) could not be explained by fractional condensation. To successfully model the observed compositions of CB chondrules, Fedkin et al. (2015) required condensation from an impact on a target differentiated into crust and mantle. Such an inherited crustal differentiation should leave distinct chemical effects in the compositions of CB silicate clasts or chondrules. The present study tests the viability of the premises of Fedkin et al. (2015) by analyzing chemical abundances in silicate clasts from the Gujba CB_a chondrite. With the exception of the study by Krot et al. (2001a) that reported major elements and REE for CB_b clasts, we are aware of only one chemical analysis of

a Gujba clast by Rubin et al. (2003), so that the present study is the most comprehensive chemical study of CB_a silicate clasts available. Elemental abundances were measured in each of the Gujba clasts by laser ablation inductively coupled plasma mass spectrometry (LA-ICP-MS), the initial results of which were presented by Oulton et al. (2015). The data are used to address issues of volatilization and chemical differentiation in the CB chondrites.

2. ANALYTICAL METHODS

Thirty-two (32) silicate clasts in nine polished slices of Gujba were studied for texture and composition. Clast petrographic types were designated based on observations procured using reflected light microscopy on a Nikon SMZ-2T optical microscope with magnification ranging from 10 to 63×. Silicate clasts in Gujba were analyzed for 53 elements using an ESI New Wave™ UP193FX excimer (193 nm) laser ablation system coupled to a Thermo Electron Element XR™ ICP-MS at the Plasma Analytical Facility of the National High Magnetic Field Laboratory (Humayun et al., 2007, 2010; Gaboardi and Humayun, 2009; Humayun, 2012; Yang et al., 2015). Clasts were analyzed using a 150 μm spot, at 50 Hz repetition rate, with a 20 s dwell time (i.e., 1000 shots per spot). A 1-s, 10 Hz pre-ablation with the same spot size was utilized to minimize surface contamination, after which a 10-s washout period was allowed before the main ablation began. Each clast was probed with 5–15 spot analyses that were averaged to produce a composition representative of the entire clast. Since the spot size employed here was larger than the grain size within the clasts, the averaged chemical analyses reported here are considered to be representative of the bulk compositions of the clasts.

Isotope peaks were collected in low-resolution with analog mode detection (for major elements) and triple-mode detection (for other measured elements). Peaks acquired are ^{7}Li, ^{9}Be, ^{11}B, ^{23}Na, ^{25}Mg, ^{27}Al, ^{29}Si, ^{31}P, ^{34}S, ^{35}Cl, ^{39}K, ^{44}Ca, ^{45}Sc, ^{47}Ti, ^{51}V, ^{53}Cr, ^{55}Mn, ^{57}Fe, ^{59}Co, ^{60}Ni, ^{63}Cu, ^{66}Zn, ^{71}Ga, ^{74}Ge, ^{75}As, ^{77}Se, ^{85}Rb, ^{88}Sr, ^{89}Y, ^{90}Zr, ^{93}Nb, ^{95}Mo, ^{138}Ba, ^{139}La, ^{140}Ce, ^{141}Pr, ^{145}Nd, ^{147}Sm, ^{153}Eu, ^{158}Gd, ^{159}Tb, ^{164}Dy, ^{165}Ho, ^{166}Er, ^{169}Tm, ^{174}Yb, ^{175}Lu, ^{180}Hf, ^{181}Ta, ^{182}W, ^{208}Pb, ^{232}Th, and ^{238}U. Potential elemental isobaric interferences are mostly avoided by choosing isotopes without overlapping mass/charge ratios. The interferences of double charged ions on Zn, Ga, Ge, As and Se isotopes were corrected by monitoring the doubly charged odd isotopes $^{137}Ba^{++}$, $^{145}Nd^{++}$, and $^{149}Sm^{++}$ (Yang et al., 2015). Peaks were monitored by electrically scanning the acceleration voltage (EScan mode) between magnet mass jumps and all peaks were acquired by peak jumping between peak tops with a 10% mass window and 50 ms of acquisition time on the peak top.

Standards used to convert ion intensity ratios to concentrations were the USGS glasses BHVO-2G, BCR-2G and BIR-1G, NIST SRM 610, the iron meteorites Hoba (IVB) and North Chile (Filomena, IIA), and NIST SRM 1263a steel. Concentrations for the four silicate glasses were obtained from the GeoREM database (Jochum et al., 2005, 2011; Jochum and Nohl, 2008) and for the three metal standards from Campbell et al. (2002) as updated in Humayun (2012). The precision of the major element analyses is ~2% (Humayun et al., 2010), and the precision is better than 2–5% for many of the trace elements and REEs, but lower for analyses at sub-ppm concentrations. Replicate analyses ($n = 16$) of the Smithsonian Institution's VG-2 MORB basalt were used to determine the precision with which Ce anomalies can be resolved (±3%), using the procedure adopted in this study. The detection limit was obtained by taking the 3σ uncertainty of the blank analyses and converting this to a concentration using the identical formalism for that of a peak.

3. RESULTS

Elemental abundances in the silicate clasts are reported in Table 1 together with clast designations. In Table 1, elements are listed in order of increasing atomic number with major elements reported in weight% (wt%) and other elements reported in parts per million (ppm). Detection limits are listed in the same units in Table 1.

3.1. Clast petrographic designation

Clast descriptions from AMNH 5020 were obtained by SEM BSE images and elemental maps. Each clast in GUJ slices that was measured by LA-ICP-MS was designated a petrographic type of either barred olivine (BO) or cryptocrystalline (CC) based on its appearance under reflected light microscopy (Table 1). During the examination the presence of visible banding within the silicate clast was the primary parameter for choosing a textural type. Cryptocrystalline textures completely lack visible bands within the clast, and ranged in color from dark blue–gray to a tannish-red indicative of weathering. Barred olivine clasts contain fibrous mineral bands approximately 5–20 μm in diameter. Interstitial material, identified as a mesostasis glass (Weisberg et al., 2001), is located between the fibers of the olivine bands. Of the 32 clasts measured, 8 clasts were designated as BO clasts and 24 clasts were designated as CC clasts.

3.2. Silicate major element chemistry

Major element compositions of the Gujba silicate clasts (Table 1) are shown in a ternary CMAS plot (Fig. 1) together with the compositions of silicate clasts from QUE 94411 and HaH 237 (Krot et al., 2001a). Silicate clasts in Gujba span a range of $CaO + Al_2O_3$ content from 6.7–28.5 wt%. Of the 32 clasts measured, only 2 clasts are observed to have $CaO + Al_2O_3$ content above 11 wt%, including GUJ 6-22a (28.51 wt%) and GUJ 3-27b (17.04 wt%). MgO content ranges from 24% to 42%, where the only sample below 34 wt% is GUJ 6-22a (24 wt% MgO). Lastly, SiO_2 content ranges from 44% to 54%. In Fig. 1, the Gujba silicate clasts plot on the trend defined by the CB_b clasts with the BO clast, GUJ 6-22a, possessing the composition most enriched in $CaO + Al_2O_3$ yet reported from a CB chondrite. Several differences between the Gujba clasts studied here and the CB_b clasts reported by Krot et al.

Table 1
Elemental compositions of Gujba silicate clasts where major elements are in weight%, trace elements in ppm, and values below detection limits italicized.

Clast	GUJ	GUJ	GUJ	GUJ	GUJ	GUJ	GUJ	AMNH	GUJ	GUJ	GUJ
Name	11-23a	4-27a	6-22a	3-08a	3-08b	3-27a	3-27b	5020c	11-23b	6-22b	6-22c
Type	BO	BO	BO	BO	BO	BO	BO	BO	CC	CC	CC
SiO_2	51.3	48.7	46.0	52.6	50.9	50.7	44.4	49.9	53.6	52.3	53.9
TiO_2	0.19	0.25	0.59	0.17	0.18	0.20	0.40	0.19	0.17	0.18	0.18
Al_2O_3	4.18	5.76	16.74	3.31	3.89	4.09	9.61	4.18	3.59	3.79	3.76
FeO_T	2.81	3.87	0.74	3.46	5.34	3.32	3.29	1.11	2.89	2.82	2.15
MnO	0.171	0.176	0.006	0.289	0.485	0.273	0.027	0.044	0.341	0.322	0.406
MgO	37.8	36.1	24.1	37.1	35.8	37.9	34.8	41.3	36.1	37.1	36.1
CaO	3.45	5.02	11.77	2.83	3.13	3.40	7.43	3.21	3.06	3.25	3.23
Na_2O	0.026	0.021	0.010	0.085	0.215	0.070	*0.004*	0.017	0.140	0.128	0.201
K_2O	0.0407	0.0225	0.0013	0.0104	0.0249	0.0100	0.0053	0.0018	0.0595	0.0083	0.016
P_2O_5	0.0013	0.0062	0.0028	0.0264	0.0069	0.0033	0.0048	0.0013	0.0013	0.0020	0.0009
S	0.063	0.057	0.015	0.080	0.037	0.053	0.024	0.020	0.063	0.065	0.075
Li	2.5	1.9	*0.1*	2.5	3.1	2.7	1.0	0.7	3.1	1.1	1.9
Be	0.118	0.176	0.507	0.057	0.043	0.067	0.082	0.061	0.071	0.111	0.112
B	1.14	1.29	1.06	0.76	0.48	0.52	0.37	2.60	1.08	0.78	0.82
Cl	242	228	257	305	262	257	224	216	245	202	167
Sc	15	18	47	16	17	18	37	17	15	16	15
V	112	111	152	98	111	113	167	114	102	115	99
Cr	4569	4826	1550	4298	5063	5164	3470	4084	4792	4818	5024
Co	4.5	13.6	3.8	20.1	42.9	9.4	16.7	0.9	8.7	1.2	1.2
Ni	51	218	37	289	661	128	202	9	109	2	5
Cu	1.7	0.7	2.7	1.3	1.0	1.2	2.3	3.3	1.8	1.8	2.6
Zn	1.6	1.5	1.7	1.9	0.6	1.0	1.3	0.9	0.8	0.6	1.8
Ga	0.049	0.073	0.153	0.179	0.107	0.244	0.242	0.106	0.169	0.067	0.079
Ge	*0.005*	*0.005*	*0.005*	0.106	0.043	0.026	0.140	*0.005*	*0.005*	*0.005*	*0.005*
As	0.025	0.016	0.017	0.060	0.016	0.017	0.008	0.005	0.019	0.012	0.008
Se	0.2	*0.1*	*0.1*	0.4	0.3	0.3	0.3	*0.1*	0.2	0.3	0.2
Rb	0.20	0.21	*0.01*	0.21	0.28	0.18	0.02	0.03	0.45	0.05	0.20
Sr	22.9	35.5	93.3	18.1	18.3	21.6	49.0	20.1	20.2	18.4	19.4
Y	3.79	5.61	12.33	3.59	3.88	4.30	9.15	4.06	3.28	3.55	3.65
Zr	9.6	14.0	34.9	9.5	10.3	10.6	23.6	11.0	8.2	8.9	9.7
Nb	0.74	1.05	3.07	0.66	0.70	0.74	1.52	0.77	0.62	0.65	0.67
Mo	0.027	0.032	0.178	0.109	0.067	0.026	0.252	0.026	0.248	0.032	0.045
Ba	7.3	29.4	24.6	23.3	6.7	27.7	25.1	7.5	8.7	6.2	6.4
La	0.69	1.13	2.90	1.02	0.71	1.59	1.51	0.70	0.56	0.60	0.69
Ce	1.82	2.91	5.23	2.78	2.06	4.21	3.74	2.07	1.49	1.57	1.75
Pr	0.27	0.41	1.03	0.35	0.27	0.45	0.60	0.29	0.23	0.24	0.26
Nd	1.37	2.04	5.01	1.60	1.32	1.96	3.23	1.43	1.17	1.21	1.29
Sm	0.45	0.66	1.51	0.45	0.43	0.57	1.08	0.48	0.38	0.40	0.42
Eu	0.17	0.25	0.70	0.15	0.16	0.20	0.39	0.17	0.13	0.15	0.15
Gd	0.61	0.93	1.87	0.50	0.54	0.76	1.43	0.60	0.54	0.57	0.60
Tb	0.11	0.16	0.33	0.10	0.11	0.14	0.28	0.12	0.10	0.10	0.10
Dy	0.76	1.15	2.26	0.67	0.75	0.93	1.93	0.83	0.66	0.71	0.73
Ho	0.16	0.24	0.48	0.15	0.16	0.20	0.42	0.18	0.14	0.15	0.16
Er	0.50	0.75	1.45	0.43	0.50	0.59	1.25	0.54	0.43	0.46	0.48
Tm	0.075	0.111	0.220	0.063	0.075	0.088	0.191	0.080	0.065	0.071	0.073
Yb	0.49	0.72	1.51	0.40	0.50	0.59	1.25	0.53	0.41	0.45	0.46
Lu	0.08	0.11	0.23	0.06	0.08	0.10	0.20	0.09	0.07	0.07	0.07
Hf	0.28	0.42	0.84	0.27	0.33	0.38	0.80	0.35	0.25	0.26	0.29
Ta	0.038	0.055	0.148	0.039	0.041	0.051	0.105	0.048	0.032	0.033	0.037
W	0.004	0.001	0.254	0.008	0.004	0.003	0.255	0.023	0.001	0.007	0.038
Pb	0.059	0.082	0.187	0.228	0.048	0.067	0.148	0.066	0.057	0.046	0.077
Th	0.080	0.125	0.310	0.103	0.088	0.099	0.205	0.096	0.068	0.071	0.111
U	0.025	0.074	0.051	0.045	0.027	0.057	0.041	0.033	0.026	0.021	0.033

Table 1 (*continued*)

Clast	GUJ	GUJ	GUJ	GUJ	GUJ	GUJ	GUJ	GUJ	GUJ	GUJ	GUJ
Name	6-22d	6-22F-1	6-22F-2	4-27b	4-27c	67a	67b	911a	911b	3-08c	3-08d
Type	CC	CC	CC	CC	CC	CC	CC	CC	CC	CC	CC
SiO_2	50.2	47.5	51.9	49.9	48.9	51.1	51.8	50.9	51.9	49.0	50.2
TiO_2	0.21	0.15	0.19	0.22	0.25	0.19	0.19	0.19	0.18	0.19	0.21
Al_2O_3	4.44	2.90	3.76	4.66	5.59	3.68	3.73	3.76	3.48	4.02	4.40
FeO_T	2.91	2.69	2.57	1.83	3.53	3.01	2.95	2.74	2.43	4.66	1.50
MnO	0.175	0.262	0.325	0.027	0.231	0.362	0.367	0.307	0.375	0.221	0.038
MgO	38.1	43.9	37.7	39.3	36.6	38.0	37.4	38.6	38.5	38.6	40.0
CaO	3.88	2.39	3.28	3.93	4.63	3.22	3.25	3.32	3.02	3.17	3.61
Na_2O	0.037	0.125	0.174	0.012	0.108	0.352	0.140	0.093	0.128	0.040	0.010
K_2O	0.0038	0.0087	0.0088	0.0714	0.0774	0.0672	0.0267	0.0163	0.0193	0.0037	0.0067
P_2O_5	0.0020	0.0029	0.0020	0.0028	0.0035	0.0035	0.0018	*0.0001*	*0.0001*	0.0047	0.0037
S	0.057	0.040	0.061	0.021	0.060	0.041	0.066	0.075	0.051	0.105	0.019
Li	1.4	1.0	1.1	0.9	2.7	1.7	3.3	5.4	8.4	1.9	1.3
Be	0.112	0.081	0.103	0.120	0.163	0.095	0.109	0.051	0.042	0.044	0.054
B	0.88	1.19	0.65	0.84	1.39	1.23	1.23	6.47	2.75	0.40	0.51
Cl	173	260	204	186	178	203	218	242	136	283	247
Sc	17	13	16	18	17	15	16	14	14	18	18
V	125	113	117	124	106	106	111	114	113	126	130
Cr	4624	4167	4997	3480	4471	4518	4901	4686	5061	4950	3673
Co	1.5	12.4	1.1	16.2	16.1	17.4	11.0	3.7	5.7	21.3	10.5
Ni	4	115	4	265	337	331	236	92	44	221	188
Cu	2.8	5.4	0.8	0.2	0.5	1.8	0.8	6.1	3.8	0.4	0.3
Zn	1.3	2.1	0.5	0.4	1.1	2.3	0.7	9.9	4.6	0.4	0.6
Ga	0.064	0.049	0.060	0.050	0.106	0.062	0.058	0.051	0.042	0.094	0.095
Ge	*0.005*	*0.005*	0.008	*0.005*	*0.005*	0.008	*0.005*	*0.005*	*0.005*	0.034	0.026
As	0.014	0.013	0.013	0.013	0.011	0.009	0.004	*0.002*	*0.002*	0.025	0.019
Se	*0.1*	*0.1*	*0.1*	*0.1*	*0.1*	*0.1*	*0.1*	*0.1*	*0.1*	0.3	0.2
Rb	0.04	0.08	0.08	0.47	0.58	0.92	0.39	0.28	0.27	0.07	0.08
Sr	22.2	13.9	19.2	18.9	31.0	22.0	21.6	25.2	21.2	18.4	19.4
Y	4.25	2.93	3.64	4.37	5.23	3.73	3.67	3.55	3.41	4.01	4.53
Zr	10.8	7.6	9.2	11.0	13.8	9.3	9.3	9.7	9.3	10.5	12.1
Nb	0.78	0.52	0.67	0.83	1.03	0.64	0.69	0.71	0.68	0.73	0.85
Mo	0.024	0.052	0.031	0.030	0.025	0.042	0.038	0.009	*0.003*	0.052	0.015
Ba	7.2	4.6	6.3	7.2	11.3	31.0	15.2	15.4	6.8	6.6	7.8
La	0.82	0.65	0.62	0.77	1.20	0.71	0.64	0.72	0.70	0.69	0.85
Ce	2.08	1.68	1.57	1.99	2.89	1.83	1.68	2.11	2.27	2.00	2.50
Pr	0.30	0.23	0.24	0.31	0.41	0.27	0.25	0.27	0.27	0.27	0.32
Nd	1.50	1.12	1.26	1.54	1.94	1.38	1.31	1.30	1.26	1.34	1.55
Sm	0.50	0.35	0.42	0.51	0.63	0.44	0.42	0.41	0.40	0.44	0.49
Eu	0.18	0.11	0.16	0.19	0.24	0.16	0.16	0.15	0.15	0.16	0.18
Gd	0.69	0.49	0.60	0.72	0.87	0.63	0.60	0.57	0.57	0.54	0.59
Tb	0.12	0.08	0.11	0.13	0.15	0.11	0.10	0.10	0.10	0.11	0.13
Dy	0.86	0.60	0.73	0.88	1.08	0.76	0.75	0.71	0.71	0.78	0.88
Ho	0.19	0.13	0.16	0.19	0.23	0.17	0.16	0.15	0.15	0.17	0.19
Er	0.57	0.39	0.49	0.58	0.70	0.49	0.49	0.46	0.46	0.51	0.58
Tm	0.084	0.059	0.074	0.089	0.105	0.076	0.074	0.068	0.068	0.076	0.083
Yb	0.55	0.39	0.48	0.58	0.69	0.49	0.48	0.45	0.46	0.51	0.56
Lu	0.09	0.06	0.08	0.09	0.11	0.08	0.08	0.07	0.07	0.08	0.09
Hf	0.33	0.24	0.28	0.33	0.41	0.28	0.29	0.29	0.30	0.33	0.38
Ta	0.041	0.030	0.036	0.043	0.055	0.038	0.036	0.038	0.037	0.042	0.050
W	0.055	0.009	0.001	0.002	0.003	0.003	0.001	0.011	0.014	0.003	0.003
Pb	0.077	0.088	0.047	0.056	0.171	0.121	0.059	0.131	0.081	0.047	0.060
Th	0.116	0.076	0.078	0.096	0.140	0.102	0.089	0.085	0.077	0.088	0.102
U	0.036	0.036	0.020	0.025	0.039	0.036	0.026	0.049	0.031	0.028	0.036

(*continued on next page*)

Table 1 (*continued*)

Clast Name Type	GUJ 3-27c CC	GUJ 3-27d CC	GUJ 3-27e CC	GUJ 5-34a CC	GUJ 5-34b CC	GUJ 5-34c CC	GUJ 5-34d CC	AMNH 5020b CC	AMNH 5020a CC	AMNH 5020d CC	Detection Limit
SiO_2	50.6	50.3	51.2	49.4	49.2	51.7	51.0	48.7	49.7	52.0	*0.005*
TiO_2	0.16	0.16	0.15	0.20	0.19	0.17	0.17	0.20	0.19	0.15	*0.0001*
Al_2O_3	3.48	3.67	3.38	4.16	3.92	3.59	3.63	4.66	4.21	3.40	*0.0002*
FeO_T	2.79	2.87	2.79	3.51	3.56	2.88	3.24	1.11	2.93	2.51	*0.0001*
MnO	0.533	0.391	0.526	0.204	0.229	0.386	0.287	0.031	0.391	0.418	*0.00001*
MgO	38.9	39.5	39.0	39.2	39.7	38.1	38.6	41.7	39.2	38.7	*0.0002*
CaO	2.90	2.94	2.75	3.26	3.12	2.91	2.97	3.53	3.16	2.61	*0.001*
Na_2O	0.585	0.129	0.074	0.044	0.068	0.171	0.058	0.020	0.156	0.127	*0.004*
K_2O	0.0344	0.0134	0.0145	0.0136	0.0037	0.0104	0.0051	0.0016	0.0047	0.0047	*0.0004*
P_2O_5	0.0022	0.0018	0.0024	0.0023	0.0022	0.0012	0.0018	0.0014	0.0047	0.0030	*0.0001*
S	0.048	0.057	0.043	0.038	0.033	0.059	0.039	0.022	0.053	0.051	*0.001*
Li	2.2	2.2	2.8	1.2	1.2	1.7	1.3	0.6	1.8	1.8	*0.1*
Be	0.034	0.036	0.033	0.052	0.044	0.045	0.040	0.061	0.052	0.044	*0.001*
B	0.51	0.55	0.78	0.62	0.49	0.43	0.44	1.57	1.93	1.51	*0.01*
Cl	255	223	222	243	175	146	132	238	282	207	*2*
Sc	20	16	15	18	17	15	16	18	18	15	*0.02*
V	104	104	116	127	129	104	119	126	115	109	*0.001*
Cr	5756	5404	5997	4960	5105	5175	5395	3584	5315	5529	*0.2*
Co	6.3	5.7	10.2	17.2	11.1	6.2	6.7	0.9	1.3	4.8	*0.01*
Ni	77	99	160	191	185	96	84	2	2	89	*0.2*
Cu	0.8	0.8	4.3	0.4	0.7	0.6	0.3	2.1	1.2	1.8	*0.01*
Zn	0.5	0.5	0.6	0.8	1.0	0.5	0.4	0.7	0.9	1.5	*0.01*
Ga	0.112	0.111	0.121	0.117	0.130	0.108	0.102	0.110	0.109	0.119	*0.001*
Ge	0.026	0.029	0.035	*0.005*	0.017	*0.005*	*0.005*	*0.005*	*0.005*	0.050	*0.005*
As	0.005	0.004	0.007	0.011	0.007	0.005	0.003	0.007	0.013	0.013	*0.002*
Se	0.2	0.2	0.3	*0.1*	*0.1*	*0.1*	*0.1*	*0.1*	*0.1*	*0.1*	*0.1*
Rb	0.28	0.17	0.22	0.33	0.08	0.18	0.11	0.05	0.04	0.06	*0.01*
Sr	18.6	18.5	16.6	22.3	19.8	18.5	18.3	22.9	19.6	15.5	*0.001*
Y	4.34	3.48	3.25	4.35	4.05	3.67	3.77	4.43	4.03	3.31	*0.0003*
Zr	10.6	9.1	8.4	11.4	10.7	9.7	9.9	12.2	14.0	9.5	*0.001*
Nb	0.62	0.64	0.60	0.77	0.74	0.67	0.69	0.85	0.72	0.60	*0.0002*
Mo	0.045	0.028	0.041	0.025	0.031	0.042	0.029	0.040	0.043	0.054	*0.003*
Ba	8.2	7.6	28.0	46.2	11.4	7.0	7.0	8.2	6.8	5.6	*0.001*
La	0.65	0.60	0.56	1.01	1.10	0.70	0.67	0.76	0.66	0.54	*0.0004*
Ce	1.68	1.75	1.64	2.54	2.82	2.06	1.95	2.22	1.81	1.57	*0.0004*
Pr	0.25	0.24	0.23	0.33	0.32	0.27	0.27	0.32	0.27	0.22	*0.0001*
Nd	1.35	1.25	1.18	1.57	1.51	1.30	1.32	1.62	1.40	1.12	*0.01*
Sm	0.45	0.41	0.38	0.49	0.46	0.42	0.43	0.52	0.47	0.37	*0.001*
Eu	0.14	0.15	0.14	0.18	0.16	0.15	0.16	0.19	0.17	0.13	*0.0004*
Gd	0.61	0.55	0.53	0.63	0.60	0.54	0.53	0.69	0.62	0.49	*0.001*
Tb	0.13	0.10	0.10	0.13	0.12	0.11	0.11	0.13	0.12	0.10	*0.0003*
Dy	0.87	0.72	0.67	0.86	0.82	0.74	0.76	0.91	0.83	0.67	*0.0003*
Ho	0.19	0.15	0.15	0.19	0.18	0.16	0.16	0.20	0.18	0.14	*0.0001*
Er	0.57	0.46	0.44	0.56	0.54	0.48	0.49	0.59	0.54	0.44	*0.0001*
Tm	0.090	0.070	0.066	0.084	0.080	0.073	0.074	0.089	0.081	0.065	*0.0002*
Yb	0.56	0.46	0.44	0.57	0.55	0.47	0.49	0.58	0.54	0.43	*0.0004*
Lu	0.09	0.07	0.07	0.09	0.09	0.08	0.08	0.09	0.09	0.07	*0.0002*
Hf	0.36	0.31	0.29	0.37	0.35	0.32	0.32	0.40	0.43	0.30	*0.0004*
Ta	0.044	0.038	0.035	0.047	0.045	0.041	0.042	0.050	0.043	0.036	*0.0003*
W	0.001	0.001	0.002	0.002	0.001	0.001	0.001	0.033	0.045	0.013	*0.0001*
Pb	0.055	0.054	0.049	0.062	0.063	0.054	0.048	0.069	0.056	0.051	*0.0002*
Th	0.088	0.081	0.079	0.103	0.095	0.087	0.087	0.103	0.095	0.072	*0.00002*
U	0.025	0.028	0.037	0.039	0.030	0.028	0.028	0.035	0.030	0.025	*0.00001*

(2001a) are observed. First, many of the Gujba BO clasts and all the Gujba CC clasts are very close to bulk carbonaceous chondritic composition, while CB_b clasts are distributed along the trend. Further, while many of the CB_b CC clasts plot towards the MgO–SiO_2 boundary in Fig. 1, depleted in refractory elements, there is no tendency towards refractory element depletion in the Gujba CC clasts. Fig. 2 shows the SiO_2/MgO ratio plotted against the CaO/MgO ratio for silicate clasts from Gujba compared with those from CB_b chondrites. This figure again

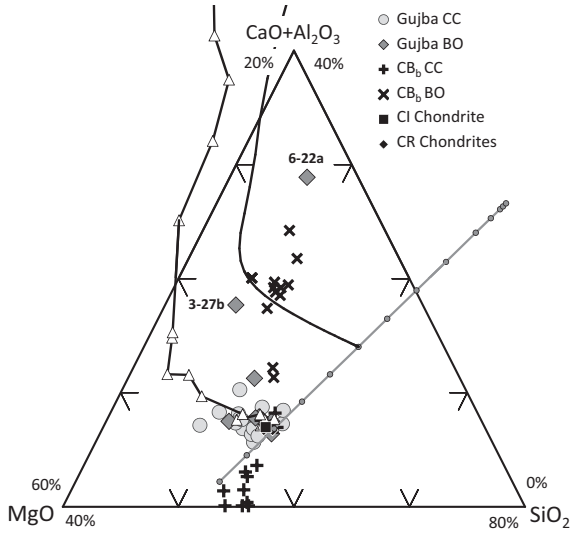

Fig. 1. Ternary plot of major element compositions of Gujba silicate clasts (this study) compared with data for CB_b silicate clasts (Krot et al., 2001a), CR chondrites (Weisberg et al., 1993) and CI chondrite (Anders and Grevesse, 1989) modified from Fedkin et al. (2015). The compositional evolution of residues of vacuum evaporation of chondritic material (Wang et al., 2001) is shown by open triangles. The modeled composition of a condensing silicate from a vapor plume produce from a differentiated CR body with a Si/H and Ni/H enrichment of 300 and 3.0×10^4 respectively, 15 wt% H_2O content, and mixing of equal proportions of mantle and crust is shown by the dotted black line crossing the CB_b compositions (Fedkin et al., 2015). The gray line shows mixing between the crust and mantle portions of a differentiated CR body (Fedkin et al., 2015), where the small gray circles mark 10% mixing intervals.

contrasts the compositional variation between Gujba clasts and CB_b clasts, where CB_b clasts define a trend of increasing SiO_2 with increasing refractory element abundance, e.g., CaO, while the Gujba clasts exhibit a large variation in SiO_2/MgO ratios at near chondritic CaO/MgO, with the notable exception of GUJ 6-22a.

3.3. Rare earth element chemistry

Concentrations of REE in Gujba silicate clasts are presented in Table 1 and CI-normalized abundances of REE concentrations are shown in Fig. 3. All clasts show an enrichment of REE relative to CI-chondrite (2.5–10×). CC clasts show concentrations 2.5–4 × CI, whereas BO clasts show concentrations 3–10 × CI. This is in contrast with REE distributions in CB_b chondrules where CC chondrules range from ~2 to 0.1 × CI, while the BO chondrules showed a similar range to Gujba BO clasts (~2–10 × CI). In addition to the range of enrichment seen in the bulk REE pattern, varying degrees of light REE (LREE) fractionation are observed in Gujba clasts. LREE fractionation is quantified by the CI-normalized La/Sm ratio, which is observed to range from 0.9 to 1.8. The middle REE patterns are flat, with a distinct HREE enrichment, $(Lu/Yb)_{CI} = 1.09 \pm 0.02$ (1σ). This distinct HREE enrichment is also seen in the Gujba silicate clast analyzed by INAA (Rubin et al., 2003).

One of the most intriguing features of the REE patterns in Gujba clasts is the presence of Ce anomalies that are resolved in over half the clasts. $(Ce/Ce^*)_{CI}$ is used to quantify the Ce anomaly where,

$$\frac{Ce}{Ce^*} = \frac{Ce}{\sqrt{(La \times Pr)_{CI}}}$$

Both positive and negative Ce anomalies are observed, the most intense of which are +22% and −25% respectively. The Ce anomalies are shown in Fig. 4 along with CB_b data (Krot et al., 2001a). There appears to be a crude correlation with CB clasts that have refractory enrichments, CaO/MgO > 0.2, having negative Ce anomalies, while clasts that

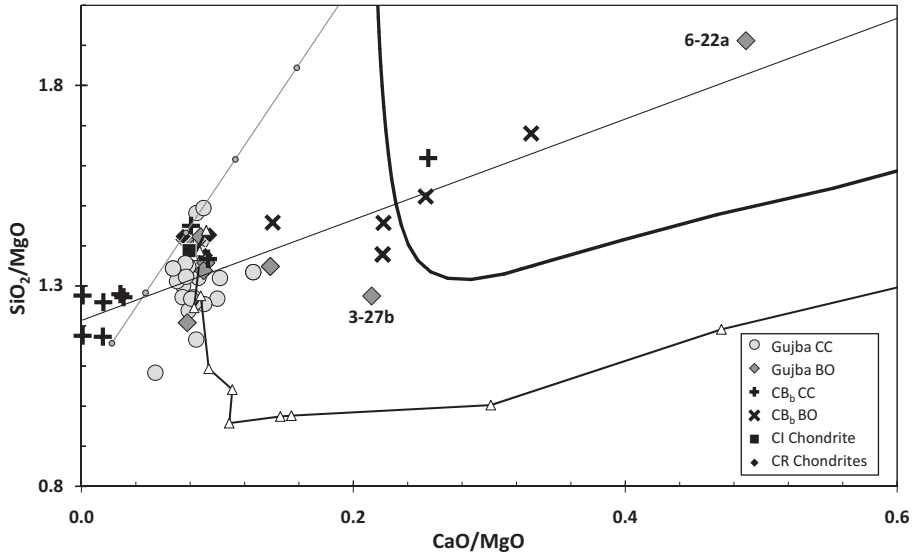

Fig. 2. CaO/MgO plotted against SiO_2/MgO for Gujba silicate clasts (this study) plotted with data for CB_b silicate clasts (Krot et al., 2001a), CR chondrites (Weisberg et al., 1993) and CI chondrite (Anders and Grevesse, 1989). Model parameters are the same as in Fig. 1. Note that variations in SiO_2 and CaO correlate. The two most refractory clasts from this study have been labeled.

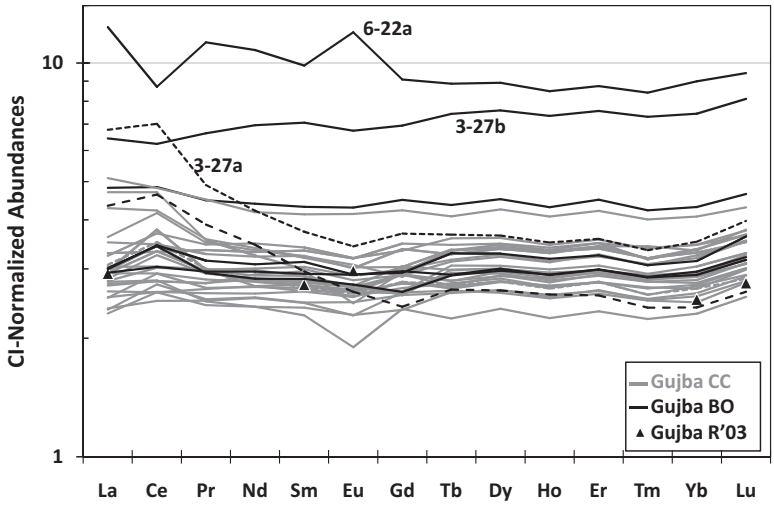

Fig. 3. CI-normalized rare earth element (REE) abundances in Gujba silicate clasts. Gujba R'03 is the silicate clast reported by Rubin et al. (2003). The dashed line is the BO clast (GUJ 3-27a) that displays strong La/Sm fractionation. Positive and negative Ce and Eu anomalies are observed. Normalizing CI abundances from Anders and Grevesse (1989).

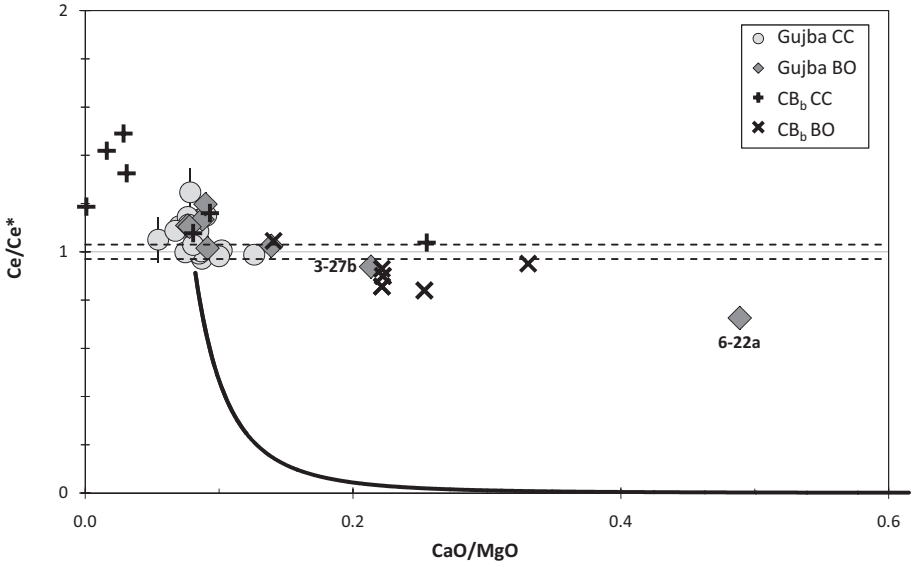

Fig. 4. The Ce anomaly for Gujba silicate clasts is plotted against the CaO/MgO ratio, along with compositions of chondrules from CB_b chondrites (Krot et al., 2001a). Dashed error bands represent the standard deviation of 16 replicate analyses of the Smithsonian MORB basalt standard (VG-2) analyzed under the same conditions as Gujba. Error bars for measured Gujba clasts are mainly smaller than the symbol size. A best-fit curve for the composition of residues of vacuum evaporation of a chondritic composition (Wang et al., 2001) is shown as the thick black curve.

are chondritic or subchondritic in refractory element abundances, CaO/MgO < 0.1, have positive Ce anomalies. Lastly, Eu anomalies are observed in many of the clasts, which range from +26% to −18%.

3.4. Refractory element chemistry

The term 'refractory elements' will be used here for elements that exhibit refractory behavior in a canonical solar nebula. Fig. 5 is a CI-normalized plot of refractory element abundances in Gujba BO and CC clasts ordered by condensation temperature in a canonical solar nebula (Lodders, 2003). Like with the REE, the refractory elements are enriched overall by an identical amount, 2.5–4 × CI with the two BO clasts similarly plotting to higher enrichments. Superposed on this general enrichment are positive anomalies in U and Ba in all the CC clasts, and many of the BO clasts, but negative anomalies in the two BO clasts with the highest enrichments of refractory elements and REEs. Refractory element relations are examined in more detail in binary plots. Fig. 6 shows the correlation between the Zr–Hf and Nb–Ta pairs. With the exception of the two

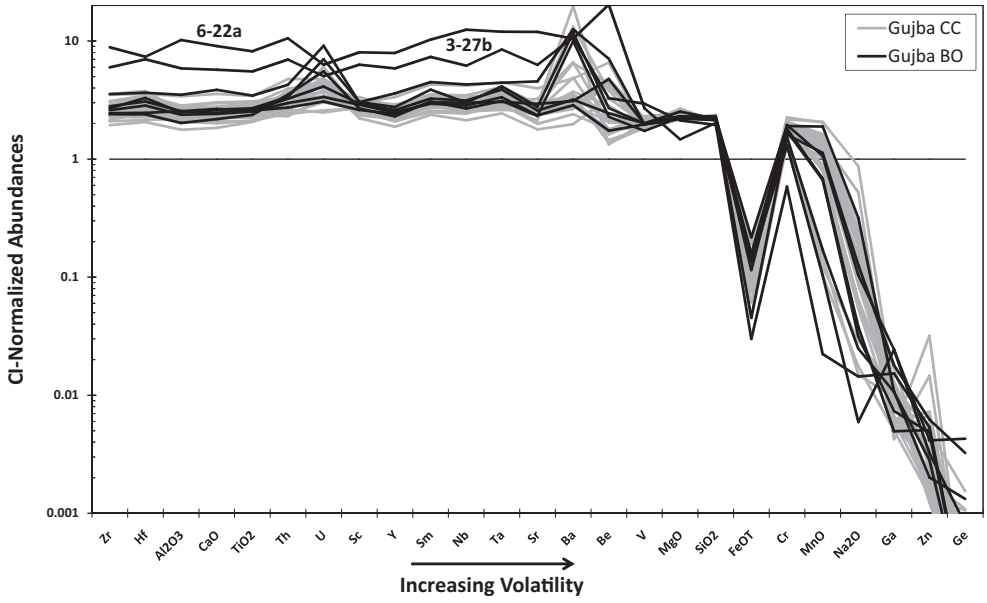

Fig. 5. Lithophile element abundances in Gujba silicate clasts (this study) normalized to CI abundances (Anders and Grevesse, 1989), except for Zr, Nb, Hf, and Ta abundances, which were normalized to CI values from Münker et al. (2003). The deficiency of Fe is due to reduction into metal. Note the presence of U and Ba anomalies in the refractory elements and the severe depletion of moderately volatile elements Ga, Zn and Ge compared with Na_2O.

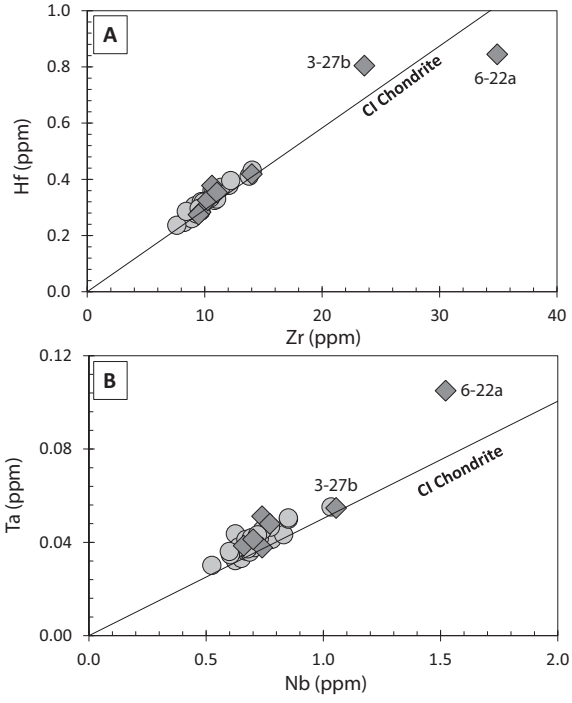

Fig. 6. Binary plots of (A) Zr vs. Hf, and (B) Nb vs. Ta, for Gujba silicate clasts. The figure legend is the same as in Fig. 4. Note the presence of large Zr/Hf and Nb/Ta fractionations in the most refractory enriched BO clasts. The CI chondrite reference values are from Münker et al. (2003).

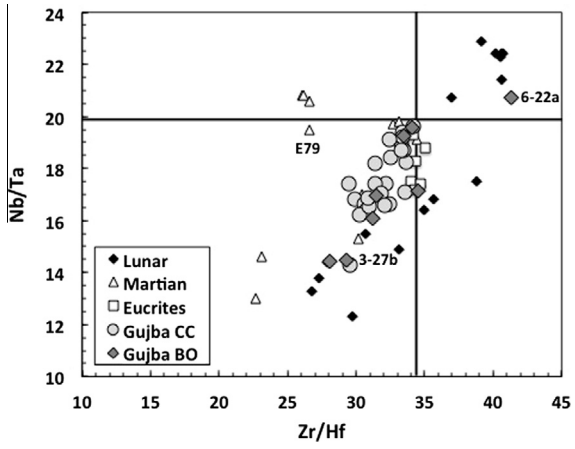

Fig. 7. Plot of Nb/Ta ratio vs. Zr/Hf ratio comparing Gujba silicate clasts with lunar, Martian and eucritic basalts, modified from Münker et al. (2003). An analysis of EETA 79001A from Yang et al. (2015) is shown as E79.

BO clasts with the highest refractory element enrichment, the CC and BO clasts exhibit chondritic Zr/Hf ratios, and slightly subchondritic Nb/Ta ratios. The two BO clasts with the highest refractory enrichment exhibit fractionated Zr/Hf ratios, each in the opposite sense, and GUJ 6-22a also has a much more subchondritic Nb/Ta ratio than the other clasts. When these relations are examined in detail by comparing the Zr/Hf ratio against the Nb/Ta ratio (Fig. 7), however, it is clear that both ratios are correlated and subchondritic in all clasts, excluding GUJ 6-22a. This is the same range as exhibited by lunar and Martian samples, and larger than the range exhibited by eucrites (Münker et al., 2003). To assess the degree to which plagioclase fractionation in the precursor may have played a role, the elements Ba and Sr are plotted against CaO in Fig. 8. The Gujba clasts exhibit a chondritic Sr/Ca ratio with the excep-

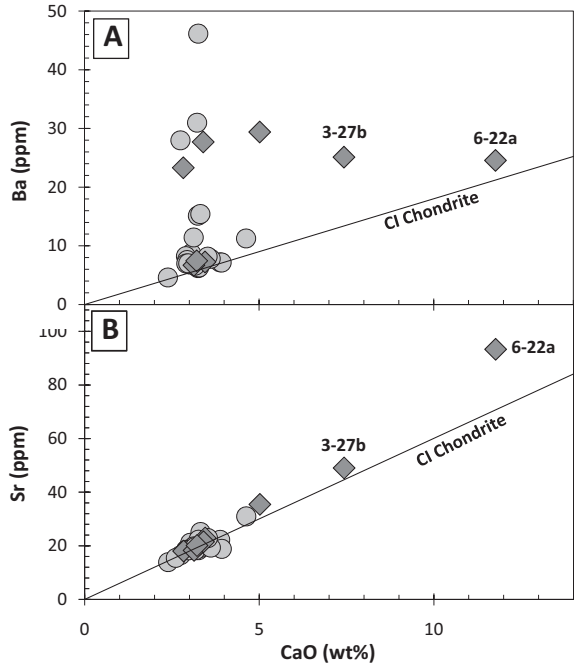

Fig. 8. Plot of (A) Ba vs. CaO, and (B) Sr vs. CaO, for Gujba silicate clasts, with CI chondrite ratios from Anders and Grevesse (1989). The figure legend is the same as in Fig. 4. Note the strong fractionations of the Ba/Ca ratio independent of the Sr/Ca ratio.

tion of GUJ 6-22a that has a superchondritic Sr/Ca ratio which, together with its positive Eu anomaly, supports a role for cumulate plagioclase in its precursor. Fig. 8 shows that the Ba/Ca ratio exhibits superchondritic values in many CC and BO clasts with Ba anomalies reaching 6 × CI, except GUJ 6-22a that has a chondritic Ba/Ca ratio. Since Ba is significantly more incompatible than Sr or Ca, in Fig. 9, Sr, Zr, Ba and U are compared with Th, an incompatible refractory element. Fig. 9 shows that Sr and Zr are correlated with Th (Fig. 9A), while Ba exhibits a similar range of variation to that observed in Fig. 8, i.e., 1–6 × CI for the Ba/Th ratio (Fig. 9B). Uranium is about as incompatible as Th, but Fig. 9B shows very significant variations of the U/Th ratio with most of the Gujba clasts exhibiting a superchondritic U/Th ratio from 1 to 3 × CI, while the two most refractory-enriched BO clasts exhibit subchondritic U/Th ratios indicating complementary losses of U from these two clasts, and significant gains of U in the other clasts. To explore the excesses or deficits of Ba and U relative to chondritic ratios, we define the Ba and U anomalies as Ba/Ba^* and U/U^*, respectively, where,

$$\frac{Ba}{Ba^*} = \frac{(Ba/Th)}{(Ba/Th)_{CI}}, \text{ and } \frac{U}{U^*} = \frac{(U/Th)}{(U/Th)_{CI}}.$$

Fig. 10 shows that, in Gujba clasts, these anomalies do not correlate mutually nor do they correlate with Ce anomalies, and this will be discussed further in a subsequent section.

3.5. Siderophile element chemistry

Fig. 5 shows that Gujba clasts exhibit strong Fe depletion (3–20% of CI abundances), due to Fe reduction into metallic clasts. The abundances of Ni are depleted in silicate

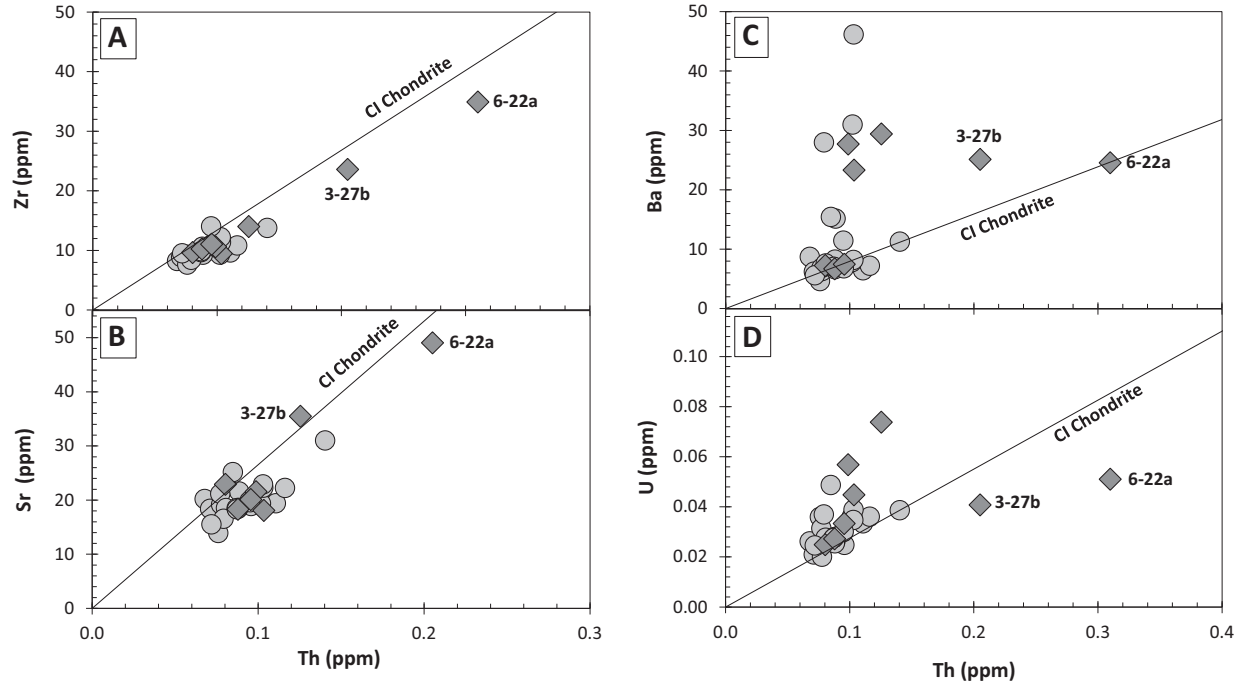

Fig. 9. Plots of refractory incompatible elements against Th for Gujba clasts, with CI values from Anders and Grevesse (1989). The figure legend is the same as in Fig. 4. (A) Zr vs. Th, note sub-chondritic Zr/Th ratio; (B) Sr. vs. Th, also sub-chondritic in Sr/Th ratio; (C) Ba vs. Th, two elements of similar incompatibility with mostly super-chondritic Ba/Th ratio; and (D) U vs. Th, exhibiting large enrichments or depletions in U relative to Th in BO clasts. Both Ba and U are volatile in oxidizing gases.

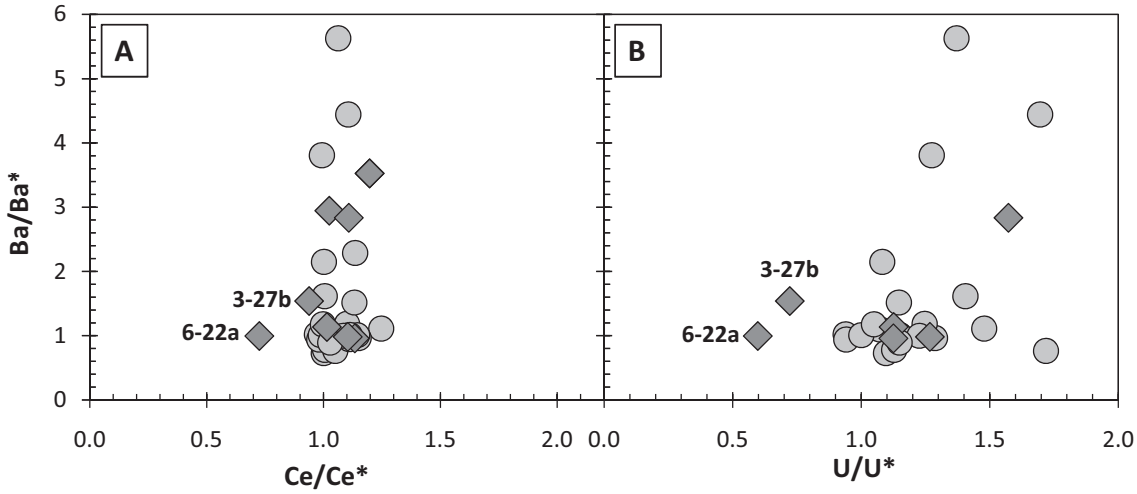

Fig. 10. Plots of refractory element anomalies for Ba against (A) Ce, and (B) U, showing little correlation between these anomalies even though all of these anomalies represent volatilization under oxidizing conditions followed by re-condensation to the cooling silicates. Particularly, the Ce anomalies are more limited in extent than the Ba and U anomalies. The figure legend is the same as in Fig. 4.

clasts to values <3%, and Co <4%, of CI abundances with the exception of GUJ 3-08b. Fig. 11A shows that there is compositional overlap between BO and CC clasts in Ni and Co content. The single silicate clast analyzed by INAA in Rubin et al. (2003) is also shown on this figure. The Co/Ni ratio is superchondritic for all clasts, but is particularly high in the clast analyzed by Rubin et al. (2003), as may be expected after metal–silicate separation. The abundances of total FeO are weakly correlated with Ni content (not shown), as well. The depletion in siderophile element content may affect the abundances of volatile siderophile or chalcophile elements, all of which are severely depleted, including Ga, As, and Ge. Surprisingly then, the abundances of V and Cr are not significantly depleted in Fig. 5. Vanadium becomes more siderophile in the presence of sulfur-rich metallic liquids, but should otherwise exhibit refractory character. If anything, V exhibits a small range of variation, unlike what is observed in refractory elements from Gujba clasts. Likewise, Cr is not significantly depleted relative to chondritic abundances. Chromium tends to be extracted into metal under reducing conditions, implying that the observed depletions are related to volatility more than to siderophile character of the elements. In contrast to the siderophile element depletions, the abundances of W range from levels typical of refractory elements (2.7 × CI) down to 0.1 × CI, uncorrelated with any other elemental variation.

3.6. Volatile element chemistry

The low volatile element abundances of Gujba clasts posed a challenge from an analytical point of view. Particularly, the abundances of alkali elements (Li, Na, K, Rb) are compromised by high and variable instrumental backgrounds that originated from ablating the standards,

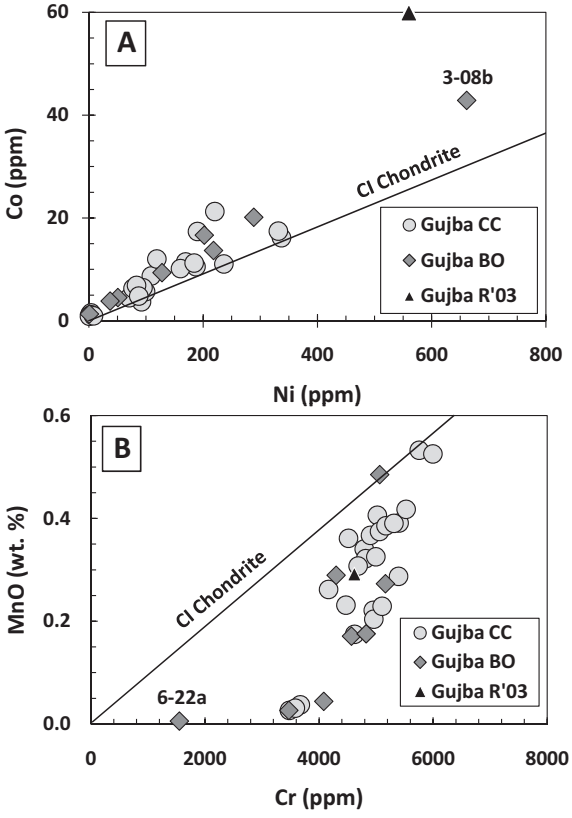

Fig. 11. Siderophile element behavior in Gujba silicate clasts in BO and CC clasts from this study (Table 1) and a clast of unspecified texture from Rubin et al. (2003). (A) Co vs. Ni, showing a superchondritic Co/Ni ratio, particularly in the clast analyzed by Rubin et al. (2003). (B) Cr vs. MnO, showing a weak correlation between Cr abundances and MnO indicating a volatile behavior of Cr. The clast from Rubin et al. (2003) plots in the middle of the Gujba clasts from this study.

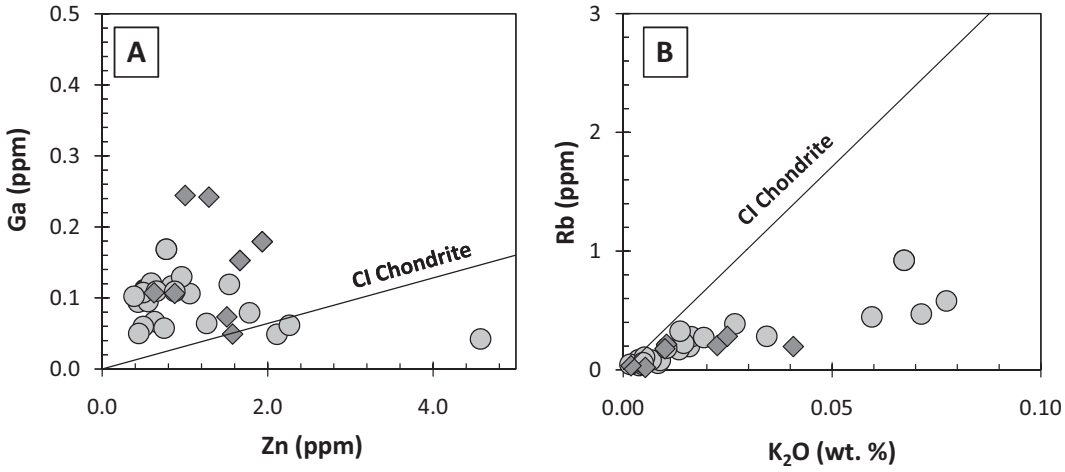

Fig. 12. Highly depleted volatile element abundances in Gujba silicate clasts, (A) Zn vs. Ga showing no correlation, but a chondritic to super-chondritic Ga/Zn ratio, and (B) K_2O vs. Rb which are correlated, with a sub-chondritic Rb/K ratio. The figure legend is the same as in Fig. 4.

particularly NIST SRM 610. Because of the instrumental blank, Cs was not detected. Fig. 5 shows that Gujba clasts exhibit strong volatile depletion, a general characteristic of CB silicate clasts. Depletions in $(Ge)_{CI}$ reach 0.001, a level rarely attained in chondrites (Weisberg et al., 1990, 2001). What is striking about the volatile depletions in Gujba silicates is that the abundances of Mn, Na and P, which are usually depleted by relatively small factors in other carbonaceous and ordinary chondrites, are so differently depleted in Gujba silicates. In both BO and CC clasts, MnO ranges from undepleted (i.e., $\sim 3 \times$ CI) to $\sim 0.5 \times$ CI, but several BO and CC clasts extend to extreme depletions of 5–50 lower than CI. For P_2O_5, most of the Gujba CC and BO clasts are depleted to <2% of CI values, the exception being GUJ 3-08a that is more volatile-rich than other clasts. With a few exceptions, Na_2O is $<0.2 \times$ CI. Correlations among the volatile elements are rather limited. The depletions of MnO and Cr are weakly correlated (Fig. 11B), indicating that volatility plays a controlling role on the Cr abundance. The Gujba clasts have higher MnO compared with CB_b chondrules, as MnO in CB_b chondrules was mostly below detection limits, <0.07 wt.% (Krot et al., 2001a). Abundances of Ga and Ge are weakly correlated, but the abundances of Ga and Zn, for example, are not correlated (Fig. 12A) even though both elements are strongly depleted. The abundances of K and Rb are correlated (Fig. 12B), but that of Na and K are not (not shown). The abundances of Pb in Gujba clasts are low, but often less depleted than Na in the same clast contrary to expectations from other chondrites or calculations of the relative volatilities of these elements in a gas of solar composition (Lodders, 2003). Likewise, the B abundance is $>0.4 \times$ CI in all clasts which makes B less depleted than Na or P. Thus, the severe volatile depletions do not follow expectations based on other chondrites or on condensation sequences from a gas of solar composition.

4. DISCUSSION

4.1. Signatures of evaporation and recondensation

During vacuum evaporation of silicate material, molecular O_2 is liberated at the surface of evaporation. This increase of O_2 sufficiently raises the fO_2 to convert the refractory Ce^{3+} to the more volatile Ce^{4+} (Wang et al., 2001). Therefore, vacuum evaporation causes Ce to be fractionated from other REE, and the resultant gas plume will be enriched in Ce relative to its companion REE. It is on this basis that clasts with negative Ce anomalies are interpreted as evaporation residues, and clasts with positive Ce anomalies are interpreted as re-condensates from the vapor plume. Davis et al. (1982) treated the issue of condensation from gases with O/H much higher than solar values using thermodynamic modeling. They found negative Ce anomalies over a broad range of oxygen fugacity above solar.

In Fig. 4, Ce anomalies for Gujba clasts and for CB_b clasts (Krot et al., 2001a) are plotted against the CaO/MgO ratio, a metric of the refractory enrichment of each clast. This plot also shows the experimentally determined trajectory of vacuum evaporation of a CI chondrite composition (Wang et al., 2001). Many of the Gujba CC and BO clasts plot near a chondritic value of the CaO/MgO ratio but exhibit positive Ce anomalies as large as 22%. This is complementary to the direction that vacuum evaporation residues follow. All the CB_b CC clasts plot from chondritic to sub-chondritic CaO/MgO ratios and exhibit strong positive Ce anomalies, while all the CB_b BO clasts are refractory enriched and exhibit negative Ce anomalies along the same trend as the two Gujba BO clasts. The CB trend is shallower than that of the vacuum evaporation residues. This is partly due to the inheritance of chemical differentiation from the target (see Section 4.2, below), which moves the clast compositions to higher CaO/MgO without any effect on the Ce anomaly. A further consideration is that the evaporative losses from CB clasts are not likely to have

occurred into vacuum. Fedkin et al. (2015) demonstrated that if the only source of oxygen in the vapor plume originated from silicate evaporation, then during recondensation the oxygen fugacity fell too rapidly to account for even the quite low FeO contents of the clasts. Their model included residual nebular gas and required the addition of significant amounts of water vapor from the impact to maintain the oxygen fugacity after condensation of most of the MgO and SiO_2. Thus, evaporation into such a reduced gas could significantly dampen the rapid loss of Ce that is observed in vacuum evaporation experiments (Wang et al., 2001). An impact plume is a distinctly non-equilibrium process where oxidizing vapor generated at silicate melt interfaces mixes with surrounding hydrogen-bearing nebular gas creating sharp gradients in oxygen fugacity. Under such conditions, volatile CeO_2 would be reduced to refractory Ce_2O_3 that would rapidly condense into the silicate melt, thereby creating positive Ce anomalies. Since the melts are expected to have initially developed negative Ce anomalies due to evaporative losses, the presence of positive Ce anomalies implies that excess Ce recondensed into those clasts. By mass balance, this requires that a substantial reservoir of clasts with negative Ce anomalies must also be present; therefore, the observed CB chondrites may have under-sampled the refractory-rich, negative Ce anomaly-bearing clasts. Bulk compositions for CB chondrites by INAA (Rubin et al., 2003) lack Ce data with which to evaluate whether there are Ce anomalies in bulk CBs.

Another surprising aspect of the Gujba clasts is the presence of ubiquitous anomalies in Ba and U abundances (Fig. 10). The relative variation in Ba abundances is about a factor of six, while that in U is about a factor of three. Of the refractory elements, the elements volatilized the most in oxidizing gases include V, Ba, Ce, W and U (e.g., Davis et al., 1982). Surprisingly, the Ba, Ce or U anomalies do not correlate with each other in Fig. 10. Vanadium depletion is implicit in the composition of GUJ 6-22a and GUJ 3-27b since both should be significantly enriched in refractory V compared with other BO and CC clasts from Gujba (Fig. 5), but the abundances of V are comparable in all the clasts. In Fig. 5, this amounts to an effective V anomaly of about three, in line with expectations from observed Ba and U depletions. Tungsten is siderophile so its depletion from the silicate clasts relative to a chondritic composition is dominated by its partitioning into metal. Campbell et al. (2002) showed that metal clasts from CB_a chondrites exhibit correlated excesses and deficits of W and Mo. Thus, five elements provide testimony to evaporation of Gujba clasts under oxidizing conditions followed by recondensation from the vapor plume. While no excesses of V are observed, U shows both deficits and excesses relative to a chondritic Th/U ratio. The Th/U ratio is not expected to fractionate significantly during melting and differentiation, so that the marked variations of the Th/U ratio observed in CB clasts (Fig. 9D) can be attributed entirely to evaporative losses from GUJ 6-22a and GUJ 3-27b, and recondensation of U-enriched gases by the other clasts. As discussed above for Ce, a mass balance problem exists with there being too few U-deficit residues and no Ba-deficit residues. Where are the complementary volatilization residues?

The extent to which GUJ 6-22a and GUJ 3-27b were volatilized can be determined from their refractory element enrichment, excluding Ba and U. The approximate level of refractory element enrichment relative to CI chondritic abundances for most Gujba clasts is about $2–3 \times$ CI (Fig. 5) that reflects the loss of highly volatile elements (mainly water, C and S) and of metal from a CI chondritic composition. GUJ 6-22a is enriched by a factor of $8–10 \times$ CI, or about 3–4 times higher than the typical CC clast composition. Thus, this most refractory enriched composition represents about 25–30% residue of volatilization, while GUJ 3-27b represents ~50% residue of volatilization relative to typical Gujba clast compositions. There are no Mg isotopic data available for these clasts, but two prior studies reported small positive or negative Mg isotope fractionations in CB chondrules with respect to Bulk Silicate Earth, consistent with evaporation/re-condensation processes occurring in a dense vapor plume (Gounelle et al., 2007; Olsen et al., 2013). It should be noted that with the exception of these two refractory-enriched clasts, the other BO and CC clasts have largely experienced recondensation of vapor from the plume. This can be observed in Fig. 2, where the SiO_2/MgO ratios for the majority of the Gujba BO and CC clasts vary along a trajectory perpendicular to the CB_b trend. It can be observed in Fig. 4, where the majority of the Gujba clasts exhibit positive Ce anomalies of varying degrees from approximately none to +22%.

4.2. Evidence for a differentiated target

The impact model proposed by Campbell et al. (2002) required a metallic impactor and a chondritic target to explain the high metal/silicate ratio in the CBs, and to explain the Pd/Ir behavior of CB metal. In canonical solar nebula conditions, Pd is about as volatile as Fe, but in CB metal Pd behaved more refractory, similar to Ir. Campbell et al. (2002) interpreted the Pd/Ir variation as the result of condensation of metal from a metal-enriched vapor plume at much higher temperatures and pressures than condensation in a canonical solar nebula. Fedkin et al. (2015) found that the compositions of the CB_b silicate clasts of Krot et al. (2001a) could not be condensed from a vapor plume formed by collision between a metal impactor and a chondritic target. Their study showed that the CB_b silicate clasts could only be fit by condensate compositions if the silicate target was differentiated into crust and mantle, and the vapor plume inherited part of the chemical heterogeneity of the target. Further, Fedkin et al. (2015) showed that the compositions of the metal clasts are permissive to a broad range of variation of the composition of the silicate target from chondritic to various types of achondrite. One of the goals of the present analytical study of Gujba silicate clasts is to examine the evidence for such differentiation. Krot et al. (2001a) did not report trace elements, other than REE, that could be used to assess evidence of differentiation in silicate clasts from CB_b chondrites so that a comparison between Gujba (CB_a) and CB_b chondrites cannot be made at present. Below, we present the chemical evidence that silicate

clasts in Gujba were inherited from a differentiated silicate precursor or protolith.

Planetary crusts are enriched in Ca, Al, Ti and Si relative to planetary mantles that contain more Mg (Taylor and McLennan, 2009). While Ca, Al and Ti are refractory elements the abundances of which correlate during evaporation and condensation processes, Fedkin et al. (2015) showed that MgO condenses before SiO_2 for all parameters explored in their models. In Fig. 2, a positive correlation between SiO_2/MgO and CaO/MgO for Gujba and CB_b clasts is observed. Also shown on this plot are the calculated compositions of the crust and mantle of a differentiated CR body and the mixing line between them. The compositional trajectory of condensates from a vapor plume of a differentiated CR body with a Si/H enrichment of 300, and Ni/H enrichment of 3.0×10^4, with 15 wt% H_2O, and mixing of equal proportions of mantle and crust is shown (Fedkin et al., 2015). The compositional trajectory of the residues of vacuum evaporation of a synthetic CI chondrite (Wang et al., 2001) is also shown. The bulk compositions of CR and CI chondrites are shown, and the Gujba clasts originate near those chondritic compositions and evolve along the line of vacuum evaporation. The compositions of silicate clasts from CB_b chondrites (Krot et al., 2001a) clearly define a trend line that neither follows the vacuum evaporation trend nor that of condensation of a dust- and ice-enriched gas, but exhibits higher SiO_2 with higher CaO. The Gujba clast, GUJ 6-22a, defines an extreme composition along this line, but the trend is defined mainly by the CB_b clasts. This relationship between CaO and SiO_2 is not a simple mixing line between crust and mantle, nor is it simply the compositional trajectory of evaporation or condensation under widely differing conditions.

The REE abundances (Krot et al., 2001a; this study) provide two additional lines of evidence for inherited differentiation. First, the CI-normalized La/Sm ratio in Gujba clasts, which quantifies the LREE fractionation, is observed to range from 0.9 to 1.8. There are no known evaporation and recondensation processes that can fractionate La/Sm to this extent. Igneous processes, though, can create this fractionation because La is more incompatible than Sm. The REE pattern of GUJ 3-27b (Table 1; Fig. 3) exhibits high REE abundances, but a LREE-depleted pattern, $(La/Sm)_{CI}$ of 0.9, reminiscent of that observed in terrestrial mid-oceanic ridge basalts of N-MORB type (Gale et al., 2013). Since the REE are incompatible elements, such a pattern represents extraction of crust from a depleted mantle, i.e., a secondary crust (Taylor and McLennan, 2009), a surprising feature for what one might assume was a small planetesimal. The clast GUJ 6-22a with the highest overall REE pattern is LREE-enriched indicating that the overall abundances are not necessarily inherited from a differentiated source, but that the shape of the REE patterns must be. For example, GUJ 3-27a is not significantly different in its overall REE pattern from Gujba CC clasts, but it exhibits the largest LREE enrichment observed with $(La/Sm)_{CI}$ of 1.8.

Second, both positive and negative Eu anomalies are observed in the Gujba clasts (Fig. 3). In reducing gases, Eu is more volatile than other REE, followed by Yb. In Gujba clasts, the observed range of the Eu anomalies is 0.85–1.33, but the majority of clasts average 0.97 ± 0.03 (1σ), so that four clasts dominate that range, including GUJ 6-22a. To assess whether this is inherited from a differentiated target or originated in the vapor plume during evaporation/recondensation processes, we next consider Yb anomalies that do not form during differentiation. The observed range of Yb anomalies is 0.86–1.01, with an average of 0.96 ± 0.02 (1σ), with only one clast (GUJ 911b) exhibiting an apparent Yb anomaly. By contrast, three of the eight BO chondrules from CB_b chondrites exhibit negative Yb anomalies (0.76–0.81) (Krot et al., 2001a). Should an evaporation event under reducing conditions have been experienced by the Gujba silicates, it is expected that more clasts would display a negative Yb anomaly. Further, evaporation under reducing conditions would produce a negative Eu anomaly in evaporation residues, but no Ce anomaly. Contrasting this, a chemically fractionated crust containing plagioclase cumulates would contain a positive Eu anomaly and high Sr abundances. The combination of a negative Ce anomaly (suggesting oxidized evaporation) with a positive Eu anomaly and no discernable Yb anomaly (e.g., GUJ 6-22a) is consistent with inheritance of the Eu anomaly from a differentiated precursor.

The relative abundances of the refractory elements, Zr, Nb, Hf and Ta should remain constant during volatilization or recondensation. Employing a precise isotope dilution technique, Münker et al. (2003) showed that different planets exhibited broad ranges in their Zr/Hf and Nb/Ta ratio due to the larger incompatibility of Nb relative to Ta and of Zr relative to Hf during partial melting of planetary mantles. Yang et al. (2015) showed that the precision of Nb/Ta and Zr/Hf ratios generated by our LA-ICP-MS technique was comparable to that of Münker et al. (2003). In Fig. 7, the Nb/Ta ratios vs. Zr/Hf ratios of Gujba clasts are compared with planetary basalt compositions from Münker et al. (2003). The Gujba clasts have Nb/Ta ratios that vary from 14 to 21, compared with eucrites (17–20), Martian meteorites (13–21) and lunar basalts (12–23). Similarly, the Zr/Hf ratios in Gujba clasts range from 29 to 41, compared with eucrites (34–35), Martian meteorites (23–34) and lunar basalts (27–41). Further, both CC and BO clasts define a correlation that passes through the chondritic reference value of Münker et al. (2003), similar to that of Martian and lunar basalts, exhibiting a larger Zr/Hf variation than eucrites. Interestingly, most of the Gujba clasts (except GUJ 6-22a) exhibit subchondritic Nb/Ta and Zr/Hf ratios indicating derivation from a depleted source, directly or indirectly. Thus, perhaps only GUJ 6-22a originated mainly by melting and evaporation of crustal rock, while the other samples contain a dominant contribution from the depleted mantle or from melting of differentiated crust that was secondary in origin, similar to basalts from the Moon, Mars and the Earth (Münker et al., 2003).

Thorium and Sc share similar highly refractory behavior, but differ the most among refractory incompatible elements in their degree of incompatibility with Th being highly incompatible while Sc is only moderately incompatible. Thus, during evaporation processes Th and Sc will not

fractionate from one another, though during igneous processes Th will partition into melts more readily than Sc. During igneous differentiation of a planetary body Th would be fractionated into a "crustal" melt component to a higher degree than Sc, resulting in a larger range in Th than Sc. Clasts measured in this study are interpreted to exhibit both features of crustal differentiation and volatilization, reflecting Gujba's complex history. Fig. 13 shows that 30 of the 32 clasts measured, both CC and BO, plot in a cluster with Sc ranging from 14.6–19.5 ppm (34% variation) and Th ranging from 0.7–0.14 ppm (100% variation). A trend for model compositions that reflect melts extracted after varying degrees of batch partial melt of a chondritic protolith is shown. Partition coefficients for the model were taken from Kennedy et al. (1993) who determined the partition coefficients of incompatible trace elements (particularly Sc) between chondritic melt and olivine, orthopyroxene and clinopyroxene. Fedkin et al. (2015) estimated the crustal composition as a 20% partial melt, which is depicted in Fig. 13 as "CR crust". The exact degree of melting assumed is not critical as the melting trend is basically horizontal. Mixtures between either bulk chondrite or residual mantle compositions (which plot near the Sc axis) will also plot along a horizontal line away from the CI trend. As such, the larger range in Th relative to Sc for Gujba clasts is consistent with the hypothesis that the silicate protolith during the CB impact event was a differentiated parent body. Similar variations are present in the Zr vs. Th and Sr vs. Th plots (Fig. 9A,B), but both Zr and Sr are more incompatible than Sc and so the differentiation effect is not as well developed as it is for Sc vs. Th.

The two clasts (GUJ 6-22a and GUJ 3-27b) that do not plot in this cluster (Fig. 13) display extreme enrichment of Th and Sc relative to the other clasts. These two clasts have displayed other chemical traits (enriched CaO, TiO_2, Al_2O_3, REEs) that have resulted in their interpretation as evaporation residues. Evaporation residues are expected to follow lines of constant Th/Sc ratio. In this context, the enriched Th and Sc can be explained as the result of evaporation of major elements (MgO and SiO_2) that would produce the enrichment of Th and Sc within the clast, but would not fractionate Th from Sc relative to the other clasts. This chemical signature is observed in Fig. 13, consistent with the hypothesis that GUJ 6-22a and GUJ 3-27b are evaporation residues. If these two clasts had originated from a chondritic starting composition, however, then their final Th/Sc would still be chondritic. The observed fractionations of Th from Sc in these two clasts had to be inherited from the cluster of compositions that exhibit evidence of inherited crustal differentiation clearly demonstrating that crustal differentiation preceded the evaporation process.

4.3. Refractory precursors to chondrules

The enrichment of refractory elements observed in silicate clasts could be due to the incorporation of debris from refractory inclusions mixing with normal chondritic matter. Misawa and Nakamura (1988) reported fractionated REE patterns, with Ce, Eu and Yb anomalies, in Allende chondrules which were considered to have originated by incorporation of refractory precursors to chondrules that had suffered high temperature nebular processing before becoming part of the chondrule (cf. Grossman and Wasson, 1983). Krot et al. (2012) proposed a link between CAIs and Al-rich chondrules in CH/CB chondrites based on the ^{16}O-depleted character of such CAIs. Although CAIs are rare in CB/CH chondrites, Krot et al. (2001a) reported chemical analyses for several inclusions. One such inclusion from HH 237, #4-1, is enriched by 100 × CI and has large negative Ce, Eu and Yb anomalies (Krot et al., 2001a). In gen-

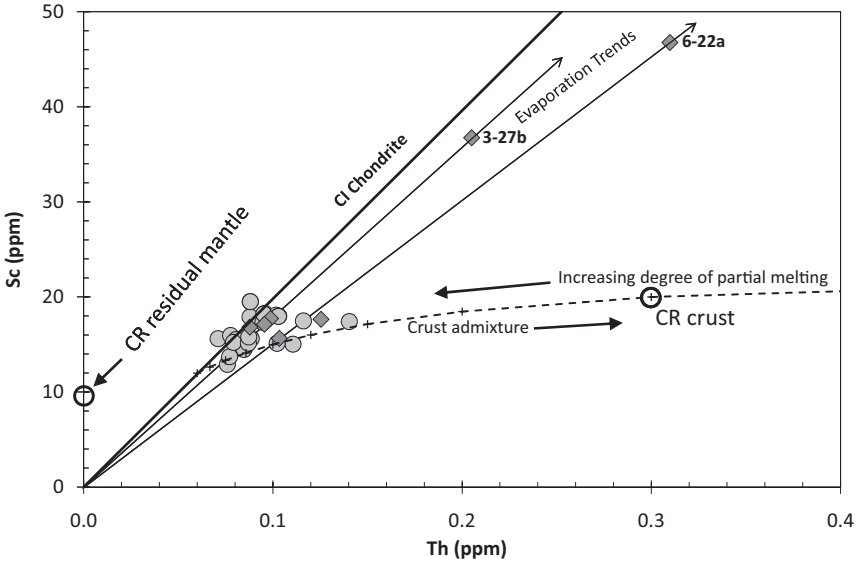

Fig. 13. Plot of Sc vs. Th in Gujba silicate clasts. The figure legend is the same as in Fig. 4. Equilibrium batch partial melts of a CR composition are shown as the dashed line, with the CR crust and residual mantle compositions of Fedkin et al. (2015). The dashed line is also parallel to a mixing line between crustal melts and mantle compositions. Evaporation trends are assumed to exhibit constant Th/Sc ratios.

eral, CAIs are enriched by ~20 × CI in refractory element abundances (Grossman, 1980). Thus, to make the refractory enrichments observed in GUJ 6-22a and GUJ 3-27b (~8–10 × CI) one would need to add ~10% of #4-1 or 50% of average CAI to normal chondritic material. One might expect that the refractory-enriched BO clasts would reflect inheritance of Ce, Eu and Yb anomalies, fractionated REE pattern or oxygen isotope ratios that were more negative than those of other chondrules from CB chondrites, but CAIs from CH/CB chondrites tend to have certain unique characteristics like ^{16}O-depletion (Krot et al., 2012) making compositional criteria a better means of approaching this issue. The refractory element patterns of Gujba silicate clasts exhibit ubiquitous Ce and Eu anomalies but little by way of resolvable Yb anomalies, and show excesses of Ba and U (excluding the two clasts discussed above) relative to other refractory elements. Such features are not known to be common in CAIs so that the CAI-mixing hypothesis finds little support in the compositions of Gujba silicate clasts. The majority of Gujba silicate clasts have chondritic CaO/MgO ratios but many of these clasts exhibit strong positive Ce anomalies (Fig. 4), but CAIs with positive Ce anomalies are not known from CB/CH chondrites, although the number of analyzed CAIs is quite small. Further, the REE patterns of Gujba clasts are largely flat with some exhibiting LREE fractionation, which is quite different from the REE patterns of Allende chondrules that resemble those of refractory inclusions (Misawa and Nakamura, 1988). However, the correlation of Sm with Ca observed by these workers led them to conclude that even for Allende chondrules, CAIs were not the refractory precursors involved.

Evidence for magmatic differentiation preceding volatilization is far more problematic for the CAI-mixing hypothesis. Fractionations of the Th/Sc, Sr/Th, Zr/Th, Zr/Hf and Nb/Ta ratios that follow characteristically magmatic patterns are not expected from CAIs. There is a caveat, however, in that published refractory element ratios in CAIs show significant variability with respect to CI ratios, e.g., $(Th/Sc)_{CI} \sim 1.4–2.3$ (Ekambaram et al., 1984). It is difficult to assess how much of this is the result of nebular processes and how much originates from unrepresentative sampling of igneous CAIs. Simon and Grossman (2004) showed that many CAIs analyzed by INAA did not show solar CaO/Al_2O_3 ratios (and by extension non-solar refractory element ratios) due to laboratory sampling artifacts. The inclusions used to obtain the Th/Sc ratio above did not have solar CaO/Al_2O_3 ratios (Ekambaram et al., 1984). We conclude that mixing of refractory precursors inherited from CAIs does not provide a compelling interpretation of compositional variation of the Gujba silicate clasts, but that the compositional variability of CAIs does not allow for a clear test of the hypothesis.

4.4. An Impact origin for chondrules

The history of ideas for impact-induced origins of chondrules is extensive (Zook, 1981; Hutchison, 1996; Sanders and Scott, 2012), but arguments against an impact origin have long prevented acceptance of this idea (Taylor et al., 1983; Zanda, 2004). In one of its more recent formulations, Sanders and Scott (2012) have argued for collisional disruption of a partially molten body. One crucial piece of evidence in favor of such a model would be chemical evidence of differentiation. The first stage of differentiation involves separation of dense metallic liquid from the molten silicate (e.g., Elkins-Tanton et al., 2011), leading to metal–silicate fractionation in chondrites. Under the assumption that such evidence would not be found, Hevey and Sanders (1996) have argued for rapid convection in the molten portion of the body so that the phase separation normally associated with metal–silicate differentiation would not occur. If the planetesimal went beyond core formation and formed a primary crust then evidence of igneous differentiation might be found in the post-impact debris, as has proven very useful in elucidating the origin of Gujba chondrules. Finally, the planetesimal may have cooled after differentiating so that solid metal separated from liquid metal in the core resulting in post-collisional evidence that could also include fractionation of Re/Os and Pt/Os in the metallic products.

Based on the higher than chondritic Re/Os ratios in ordinary chondrite (OC) metal, Chen et al. (1998) proposed that fractional crystallization in a planetesimal core had taken place followed by disruption and redistribution of the metal into ordinary chondrites. The high Re/Os ratios of OC metal were investigated in more detail by Humayun and Campbell (2002), who found that W and Re had diffused from the matrix into metal during reduction accompanying metamorphism. Early hints of differentiation in bulk OC chondrule compositions (Gooding et al., 1980) were re-interpreted by subsequent workers (Grossman and Wasson, 1983) as distinct refractory components formed by nebular condensation. Alexander (1994) analyzed the lithophile element compositions of OC chondrules and concluded that many chondrules must have formed by recycling of earlier generations of chondrules because igneous differentiation effects (compatible–i ncompatible element fractionation) could be discerned within OC chondrules. Particularly, lithophile incompatible elements are concentrated into chondrule glass so that if first-generation chondrules are fragmented and the debris is recombined randomly into next-generation chondrules, then this inherited chondrule glass creates a small magmatic differentiation effect in chondrules (Alexander, 1994). Such an effect is difficult to distinguish from the differentiation effects described above for Gujba CB clasts, limiting even some of the chemical tracers that may be used to probe an impact melting origin of OC chondrules. Hutchison (1996) reviewed evidence for the presence of igneous objects within ordinary chondrites and advocated for the role of planetary differentiates within chondrites. The issue of differentiation prior to chondrule formation deserves to be revisited from new analytical and theoretical perspectives obtained from this study.

Horstmann et al. (2014) found that the main form of metal occurrence in enstatite chondrites, metal-sulfide nodules, had magmatic differentiation patterns in their highly siderophile element abundances (see also van Niekirk et al., 2009), implying an origin by impact melting of a

differentiated source. Thus, while no unambiguous evidence for an impact origin of metal in OC chondrules is known, there is strong evidence in primitive enstatite chondrites for an origin of metallic nodules by impact melting. Like CBs, EL3 chondrites contain essentially metal-free silicate chondrules and metallic nodules. The lithophile element systematics of E3 chondrites needs to be investigated similarly to the methods used above to ascertain whether E3's record igneous fractionations or volatile fractionations that are imposed on igneous differentiation.

Among carbonaceous chondrites, only the CBs have shown strong evidence for an impact origin, e.g., the superchondritic metal–silicate ratio. This may extend to include CH chondrites as Wasson and Kallemeyn (1990) argued for an impact origin of the CH chondrite ALH 85085 and Krot et al. (2007) argued for an impact origin of CH/CB-like chondrules in Isheyevo. Based on their ^{16}O-depleted compositions, Krot et al. (2012) argued that CAIs in CB and CH chondrites equilibrated with an impact vapor plume. Campbell and Humayun (2004) cast the origin of the zoned and unzoned metal in CH chondrites within a nebular setting, similar to that for CB_b metal (Campbell et al., 2001), but Fedkin et al. (2015) showed that both types of CB metal are consistent with formation inside an impact plume. Evidence of volatilization/recondensation processes is abundant in CR chondrite metal (Connolly et al., 2001; Zanda et al., 2002; Humayun, 2012), but no evidence of prior differentiation has been reported in chondrules or metal from CR chondrites. Alexander et al. (2008) showed that Na retention in OC and CC chondrules required solid densities in chondrule-forming regions to be sufficiently high that these regions would be self-gravitating leading to rapid accretion of chondrules. Thus, while impacts on differentiated bodies should be recognized from their chemical record, impacts on undifferentiated bodies may be harder to distinguish from the chemical consequences of other models of chondrule formation that might be equally successful at interpreting the cooling rates of chondrules (Desch and Connolly, 2002; Desch et al., 2012). Nonetheless, if clasts from CBs are not to be dismissed as a unique phenomenon that only superficially resemble chondrules, careful studies of the compositions of chondrules need to be performed to determine whether chondrules from other carbonaceous chondrites also originated by condensation from impact-induced vapor plumes. Sodium retention by porphyritic chondrules (Alexander et al., 2008), that form the majority of OC chondrules, has been shown to be consistent with an impact origin (Fedkin and Grossman, 2013), justifying a broader search for clues to precursors.

The character of the impact that generated CB metal and silicate clasts, a hyper-velocity impact by a metallic body on a differentiated body with crust, mantle and core (Fedkin et al., 2015) is very different in character than those envisaged in the most popular impact models (Sanders and Scott, 2012). For example, the target is not inferred to be molten at the time of the impact. Instead, the target is inferred to have experienced differentiation nearly as extensive as that of a planet. There is also the possibility that multiple lithologies were sampled among the silicate clasts, including plagioclase cumulates and secondary crustal rocks. In such an instance, the energy for melting and vaporization must be supplied entirely by the impactor. The 5 Ma post-CAI age of CB chondrules (Krot et al., 2005) is consistent with this scenario in that the ^{26}Al heat source that plays an important role in melting the precursor bodies (Hevey and Sanders, 2006) is extinct at the time of the CB impact event. Ahrens and O'Keefe (1972) calculated that the energy per unit mass required to melt and vaporize silicate targets impacted by metallic impactors required velocities of 7–11 km/s. This estimate is surprisingly large and requires either planet-sized bodies to be involved in the CB impact if the impact velocities are governed by their mutual escape velocities or it requires smaller bodies (of unspecified initial masses) that were scattered by planet-sized bodies so that most of the kinetic energy is supplied by the high pre-encounter velocities of the bodies. Either way, planets had to be involved, so that the 5 Ma chondrule age of CBs is indirect chronometric evidence for the first planets.

Finally, the model that successfully explains the compositions of CB metal and silicate clasts, which constitute the majority of a CB chondrite, does not explain the compositions of refractory inclusions and chondritic lithic clasts from CB chondrites. CAIs from the CB chondrites exhibit a narrow range of Δ^{17}O and a mineralogical continuity with Al-rich chondrules, which has been interpreted as evidence of refractory precursors from the debris disk surrounding the Sun (at ~5 Ma) being reprocessed within the impact plume (Krot et al., 2012). Fine-grained chondritic lithic clasts, including hydrated clasts (Bonal et al., 2010a), and anhydrous clasts containing ^{15}N-anomalies (Bonal et al., 2010b) were interpreted to have been added late to the CB body (Bonal et al., 2010b). Thus, a more comprehensive model might also include a CR-like chondritic regolith on one or both of the impactors, and material accreted from the debris disk, that contribute to the abundant diversity of clasts and inclusions found in the CB chondrites.

5. CONCLUSIONS

In this study, we have provided the most detailed chemical compositions yet reported for silicates from a CB chondrite. Gujba (CB_a) BO and CC clasts display a compositional overlap to an extent that is not seen in the CB_b subgroup where BO chondrules are distinctly refractory-enriched, of which we report only two such clasts from Gujba (GUJ 6-22a and GUJ 3-27b). None of the Gujba CC clasts exhibit the refractory element depletion observed in CC clasts from the CB_b subgroup. These differences aside, the 32 Gujba silicate clasts analyzed in this study plot on the same major element trend defined by CB_b chondrules.

Silicate clasts in Gujba contain chemical signatures inherited from the silicate planetesimal protolith proposed to have been involved in the impact event, as well as chemical signatures from the volatilization of material that occurred during the impact event. The REE patterns for Gujba silicate clasts exhibit clearly resolved cerium anomalies, both positive and negative that are unambiguous

evidence for evaporation and re-condensation processes under conditions more oxidizing than solar. Two BO clasts with negative Ce anomalies are interpreted as evaporation residues and the other BO and CC clasts with positive Ce anomalies are interpreted as droplets re-condensed from a vapor plume enriched in Ce and other volatilized elements. The two BO clasts with the highest refractory element enrichment, and negative Ce anomalies, also exhibit depletion in U relative to Th, while other silicate clasts are enriched in U relative to Th (factors of >1–3 × CI) and all clasts are enriched in Ba relative to Th (factors of >1–6 × CI). The chemical anomalies in Ba, Ce and U do not mutually correlate, and indicate that these elements were re-condensed at different rates by Gujba silicate clasts. Further, the refractory residues to the evaporation process are under-represented among the Gujba clasts.

Chondritic compositions lose SiO_2 during evaporation before a significant increase in CaO/MgO begins, and condensation reverses this trend. It is, therefore, surprising that major element compositions of CB_b chondrules (Krot et al., 2001a) and Gujba silicate clasts (this study) form a linear array in SiO_2/MgO vs. CaO/MgO, a feature characteristic of crustal rocks, inconsistent with an evaporation/re-condensation signature. To find corroborating evidence of prior chemical differentiation in the target proposed by Fedkin et al. (2015), we examined inter-element variations in highly refractory elements like Sc, Zr, Nb, REE, Hf, Ta and Th, which differ significantly in compatibility during differentiation. REE patterns show variable degrees of LREE enrichment and depletion, $(La/Sm)_{CI}$ ratio of 0.9–1.8, that can only be achieved as products of an igneous event. Eu anomalies are also observed and are thought to have been possibly inherited from a differentiated crust containing lithologies with plagioclase cumulates or a lack thereof. The most distinctive differentiation effects are seen in the geochemically similar pairs Nb/Ta vs. Zr/Hf, and in Th-Sc plots. The Nb/Ta and Zr/Hf ratios of the Gujba clasts define a correlated trend that is similar in magnitude to what is observed in lunar and Martian basalts, and larger than the variation known among eucrites (Münker et al., 2003). Evidence for prior chemical differentiation in Gujba clasts is clearly observed on a Th vs. Sc plot, two highly refractory elements where Sc is moderately incompatible while Th is highly incompatible in silicate differentiation. The Gujba clasts exhibit a range from chondritic to higher than chondritic Th/Sc ratios plotting along a mixing trend between a putative crustal composition formed by ~20% partial melting of a CR-like body and a chondritic composition (Fedkin et al., 2015). The two most refractory-enriched clasts in Gujba also exhibit variable and high Th/Sc ratios, consistent with their derivation by evaporation from an originally heterogeneous population characterized by magmatic variations of Th/Sc, clearly showing that the chemical differentiation preceded the volatilization event. What is interesting is that none of the Gujba silicate clasts plot towards the mantle end-member of the mixing trend, i.e., have mixed a higher proportion of mantle than crust relative to a chondritic composition. There are no Sc, Zr, Nb, Hf, Ta or Th abundances available on the CB_b chondrules, but CB_b CC chondrules plot to sub-chondritic CaO/MgO and may be expected to exhibit complementary trends to those of CB_b BO chondrules.

Both the volatilization and differentiation recorded by Gujba silicate clasts are difficult to reconcile with a model where CAI debris is mixed into chondritic material or into vapor condensates from an impact onto chondritic, undifferentiated material. The reported bulk chemical compositions of CAIs suffer, however, from sampling artifacts that make testing the hypothesis problematic.

The results of this study corroborate the model of Fedkin et al. (2015) that silicate clasts in CBs originated as products of the re-condensation of vapor from an impact plume onto a differentiated target. Additionally, the new evidence shows that evaporation residues survived the impact, and that the vapor plume was enriched in the volatilized constituents of chondritic matter, including Ba, Ce and U (even though depleted in volatile elements like Ga, Ge and Zn). The metal clasts in Gujba and other CBs exhibit correlated W/Ir vs. Mo/Ir ratios, Ni zoning within CB_b metal, and Pd/Ir fractionation in Gujba metal that require formation within an impact plume (Meibom et al., 2000; Krot et al., 2001b; Campbell et al., 2002, 2005). Our work shows that both metal and silicate clasts from CB chondrites experienced similar histories in the impact plume.

Impact processes may have played an important role in the formation of chondrules, in general, although the extent of this process has yet to be fully established. Evidence of prior chemical differentiation in chondrules from ordinary chondrites has been explained as the result of chondrule recycling (Alexander, 1994), but may have been due to collisions between a chondritic impactor and a differentiated target. The presence of an abundance of differentiated bodies during the epoch of chondrule formation (e.g., Kleine et al., 2009) implies that many collisions between differentiated bodies may have taken place. Complete remixing of these bodies would be required to return primordial compositions from these collisions. The ubiquitous metal–silicate variations observed in ordinary and enstatite chondrites could have been created in impacts that left a significant portion of the target or impactor bodies intact to be preserved as achondrites or iron meteorites in the record.

ACKNOWLEDGEMENTS

We thank Eric Twelker for providing the GUJ slices, and Denton Ebel, Shawn Wallace and Mike Weisberg for providing AMNH 5020 together with SEM BSE images and chemical maps. We thank Ursula Humayun for the loan of GUJ 4-27. This research was supported by Grants NNX13AI06G (MH) and NNX13AE73G (AF and LG) from the NASA Cosmochemistry program. We thank Shuying Yang for sharing the VG-2 MORB Ce anomaly measurements, and for support with the LA-ICP-MS. We thank Sasha Krot for discussions on the origin of the CBs, editorial handling and for his comments on this manuscript. The manuscript also benefitted from comments by an anonymous reviewer.

REFERENCES

Ahrens T. J. and O'Keefe J. A. (1972) Shock melting and vaporization of lunar rocks and minerals. *Moon* **4**, 214–249.

Alexander C. M. O'D. (1994) Trace element distributions within ordinary chondrite chondrules: implications for chondrule formation conditions and precursors. *Geochim. Cosmochim. Acta* **58**, 3451–3467.

Alexander C. M. O'D., Grossman J. N., Ebel D. S. and Ciesla F. J. (2008) The formation conditions of chondrules and chondrites. *Science* **320**, 1617–1619.

Amelin Y., Krot A. N., Hutcheon I. D. and Ulyanov A. A. (2002) Lead isotopic ages of chondrules and calcium-aluminum-rich inclusions. *Science* **297**, 1678–1683.

Anders E. and Grevesse N. (1989) Abundances of the elements: meteoritic and solar. *Geochim. Cosmochim. Acta* **53**, 197–214.

Asphaug E., Jutzi M. and Movshovitz N. (2011) Chondrule formation during planetesimal accretion. *Earth Planet. Sci. Lett.* **308**, 369–379.

Bonal L., Huss G. R., Krot A. N. and Nagashima K. (2010a) Chondritic lithic clasts in the CB/CH-like meteorite Isheyevo: fragments of previously unsampled parent bodies. *Geochim. Cosmochim. Acta* **74**, 2500–2522.

Bonal L., Huss G. R., Krot A. N., Nagashima K., Ishii H. A. and Bradley J. P. (2010b) Highly ^{15}N-enriched chondritic clasts in the CB/CH-like meteorite Isheyevo. *Geochim. Cosmochim. Acta* **74**, 6590–6609.

Campbell A. J. and Humayun M. (2004) Formation of metal grains in the CH chondrites ALH 85085 and PCA 91467. *Geochim. Cosmochim. Acta* **68**, 3409–3422.

Campbell A. J., Humayun M., Meibom A., Krot A. N. and Keil K. (2001) Origin of zoned metal grains in the QUE94411 chondrite. *Geochim. Cosmochim. Acta* **65**, 163–180.

Campbell A. J., Humayun M. and Weisberg M. K. (2002) Siderophile element constraints on the formation of metal in the metal-rich chondrites Bencubbin, Weatherford, and Gujba. *Geochim. Cosmochim. Acta* **66**, 647–660.

Campbell A. J., Humayun M. and Weisberg M. K. (2005) Compositions of zoned and zoned metal in the CBb chondrites Hammadah al Hamra 237 and Queen Alexandra Range 94627. *Meteorit. Planet. Sci.* **40**, 1131–1148.

Carpozen L., Weiss B. P., Elkins-Tanton L. T., Shuster D. L., Ebel D. and Gattacceca J. (2011) Magnetic evidence for a partially differentiated carbonaceous chondrite parent body. *Proc. Natl. Acad. Sci.* **108**, 6386–6389.

Chen J. H., Papanastassiou D. A. and Wasserburg G. J. (1998) Re-Os systematics in chondrites and the fractionation of the platinum group elements in the early solar system. *Geochim. Cosmochim. Acta* **62**, 3379–3392.

Connolly, Jr., H. C., Huss G. R. and Wasserburg G. J. (2001) On the formation of Fe–Ni metal in Renazzo-like carbonaceous chondrites. *Geochim. Cosmochim. Acta* **65**, 4567–4588.

Davis A. M., Tanaka T., Grossman L., Lee T. and Wasserburg G. J. (1982) Chemical composition of HAL, an isotopically-unusual Allende inclusion. *Geochim. Cosmochim. Acta* **46**, 1627–1651.

Desch S. J. and Connolly, Jr., H. C. (2002) A model of the thermal processing of particles in solar nebula shocks: application to the cooling rates of chondrules. *Meteorit. Planet. Sci.* **37**, 183–207.

Desch S. J., Morris M. A., Connolly, Jr., H. C. and Boss A. P. (2012) The importance of experiments: constraints on chondrule formation models. *Meteorit. Planet. Sci.* **47**, 1139–1156.

Ekambaram V., Kawabe I., Tanaka T., Davis A. M. and Grossman L. (1984) Chemical compositions of refractory inclusions in the Murchison C2 chondrite. *Geochim. Cosmochim. Acta* **48**, 2089–2105.

Elkins-Tanton L. T., Weiss B. P. and Zuber M. T. (2011) Chondrites as samples of differentiated planetesimals. *Earth Planet. Sci. Lett.* **305**, 1–10.

Fedkin A. V. and Grossman L. (2013) Vapor saturation of sodium: key to unlocking the origin of chondrules. *Geochim. Cosmochim. Acta* **112**, 226–250.

Fedkin A. V., Grossman L., Ciesla F. J. and Simon S. B. (2012) Mineralogical and isotopic constraints on chondrule formation from shock wave thermal histories. *Geochim. Cosmochim. Acta* **87**, 81–116.

Fedkin A. V., Grossman L., Humayun M., Simon S. B. and Campbell A. J. (2015) Condensates from vapor made by impacts between metal-, silicate-rich bodies: comparison with metal and chondrules from CB chondrites. *Geochim. Cosmochim. Acta* **164**, 236–261.

Franchi I. A., Wright I. P. and Pillinger C. T. (1986) Heavy nitrogen in Bencubbin – A light-element isotopic anomaly in a stony-iron meteorite. *Nature* **323**, 138–140.

Gaboardi M. and Humayun M. (2009) Elemental fractionation during LA-ICP-MS analysis of silicate glasses: implications for matrix-independent standardization. *J. Anal. At. Spectrom.* **24**, 1118–1197.

Gale A., Dalton C. A., Langmuir C. H., Su Y. and Schilling J.-G. (2013) The mean composition of oceanic ridge basalts. *Geochem. Geophys. Geosyst.* **14**, 489–518.

Gooding J. L., Keil K., Fukuoka T. and Schmitt R. A. (1980) Elemental abundances in chondrules from unequilibrated chondrites: evidence for chondrule origin by melting of pre-existing materials. *Earth Planet. Sci. Lett.* **50**, 171–180.

Gounelle M., Young E. D., Shahar A., Tonui E. and Kearsley A. (2007) Magnesium isotopic constraints on the origin of CB_b chondrites. *Earth Planet. Sci. Lett.* **256**, 521–533.

Grossman L. (1980) Refractory inclusions in the Allende meteorite. *Ann. Rev. Earth Planet. Sci.* **8**, 559–608.

Grossman J. N. and Wasson J. T. (1983) Refractory precursor components of Semarkona chondrules and the fractionation of refractory elements among chondrites. *Geochim. Cosmochim. Acta* **47**, 759–771.

Hevey P. J. and Sanders I. S. (2006) A model for planetesimal meltdown by ^{26}Al and its implications for meteorite parent bodies. *Meteoritics Planet. Sci.* **41**, 95–106.

Horstmann M., Humayun M. and Bischoff A. (2014) Clues to the origin of metal in Almahata Sitta EL and EH chondrites and implications for primitive E chondrite thermal histories. *Geochim. Cosmochim. Acta* **140**, 720–744.

Humayun M. (2012) Chondrule cooling rates inferred from diffusive profiles in metal lumps from the Acfer 097 CR2 chondrite. *Meteorit. Planet. Sci.* **47**, 1191–1208.

Humayun M. and Campbell A. J. (2002) The duration of ordinary chondrite metamorphism inferred from tungsten microdistribution in metal. *Earth Planet. Sci. Lett.* **198**, 225–243.

Humayun M., Simon S. B. and Grossman L. (2007) Tungsten and hafnium distribution in calcium–aluminum inclusions (CAIs) from Allende and Efremovka. *Geochim. Cosmochim. Acta* **71**, 4609–4627.

Humayun M., Davis F. A. and Hirschmann M. M. (2010) Major element analysis of natural silicates by laser ablation ICP-MS. *J. Anal. At. Spectrom.* **25**, 998–1005.

Hutchison R. (1996) Chondrules and their associates in ordinary chondrites: a planetary connection? In *Chondrules and the Protoplanetary Disk* (eds. R. H. Hewins, R. H. Jones and E. R. D. Scott). Cambridge University Press, Cambridge, UK, pp. 311–318.

Jochum K.-P. and Nohl U. (2008) Reference materials in geochemistry and environmental research and the GepREM database. *Chem. Geol.* **253**, 50–53.

Jochum K.-P., Willbold M., Raczek I., Stoll B. and Herwig K. (2005) Chemical characterisation of the USGS reference glasses GSA-1G, GSC-1G, GSD-1G, GSE-1G, BCR-2G, BHVO-2G

and BIR-1G using EPMA, ID-TIMS, ID-ICP-MS and LA-ICP-MS. *Geostand. Geoanal. Res.* **29**, 285–302.

Jochum K.-P., Weis U., Stoll B., Kuzmin D., Yang Q., Raczek I., Jacob D. E., Stracke A., Birbaum K., Frick D. A., Günther D. and Enzweiler J. (2011) Determination of reference values for NIST SRM 610–617 glasses following ISO guidelines. *Geostand. Geoanal. Res.* **35**, 397–429.

Kallemeyn G. W., Boynton W. V., Willis J. and Wasson J. T. (1978) Formation of the Bencubbin polymict meteoritic breccia. *Geochim. Cosmochim. Acta* **42**, 507–515.

Kennedy A. K., Lofgren G. E. and Wasserburg G. J. (1993) An experimental study of trace element partitioning between olivine, orthopyroxene and melt in chondrules: equilibrium values and kinetic effects. *Earth Planet. Sci. Lett.* **115**, 177–195.

Kleine T., Touboul M., Bourdon B., Nimmo F., Mezger K., Palme H., Jacobsen S. B., Yin Q.-Z. and Halliday A. N. (2009) Hf-W chronology of the accretion and early evolution of asteroids and terrestrial planets. *Geochim. Cosmochim. Acta* **73**, 5150–5188.

Krot A. N., McKeegan K. D., Russell S. S., Meibom A., Weisberg M. K., Zipfel J., Krot T. V., Fagan T. J. and Keil K. (2001a) Refractory calcium–aluminum-rich inclusions and aluminum-diopside-rich chondrules in the metal-rich chondrites Hammadah al Hamra 237 and Queen Alexandra Range 94411. *Meteorit. Planet. Sci.* **36**, 1189–1216.

Krot A. N., Meibom A., Russell S. S., Alexander C. M. O'D., Jeffries T. E. and Keil K. (2001b) A new astrophysical setting for chondrule formation. *Science* **291**, 1776–1779.

Krot A. N., Meibom A., Weisberg M. K. and Keil K. (2002) The CR chondrite clan: implications for the early solar system. *Meteorit. Planet. Sci.* **37**, 1451–1490.

Krot A. N., Amelin Y., Cassen P. and Meibom A. (2005) Young chondrules in CB chondrites from a giant impact in the early Solar System. *Nature* **436**, 989–992.

Krot A. N., Ivanova M. A. and Ulyanov A. A. (2007) Chondrules in the CB/CH-like carbonaceous chondrite Isheyevo: evidence for various chondrule-forming mechanisms and multiple chondrule generations. *Chem. Erde* **67**, 283–300.

Krot A. N., Nagashima K. and Petaev M. I. (2012) Isotopically uniform, ^{16}O-depleted calcium, aluminum-rich inclusions in the CH and CB carbonaceous chondrites. *Geochim. Cosmochim. Acta* **83**, 159–178.

Lodders K. (2003) Solar system abundances and condensation temperatures of the elements. *Astrophys. J.* **591**, 1220–1247.

Lugmair G. W. and Shukolyukov A. (2001) Early solar system events and timescales. *Meteorit. Planet. Sci.* **36**, 1017–1026.

Meibom A., Desch S. J., Krot A. N., Cuzzi J. N., Petaev M. I., Wilson L. and Keil K. (2000) Large-scale thermal events in the solar nebula: evidence from FeNi metal grains in primitive meteorites. *Science* **288**, 839–841.

Misawa K. and Nakamura N. (1988) Demonstration of REE fractionation among individual chondrules from the Allende (CV3) chondrite. *Geochim. Cosmochim. Acta* **52**, 1699–1710.

Morris M. A. and Desch S. J. (2010) Thermal histories of chondrules in solar nebula shocks. *Astrophys. J.* **722**, 1474–1494.

Münker C., Pfänder J. A., Weyer S., Büchl A., Kleine T. and Mezger K. (2003) Evolution of planetary cores and the Earth–Moon system from Nb/Ta systematics. *Science* **301**, 84–87.

Newsom H. E. and Drake M. J. (1979) The origin of metal clasts in the Bencubbin meteoritic breccia. *Geochim. Cosmochim. Acta* **43**, 689–707.

Olsen M. B., Schiller M., Krot A. N. and Bizzarro M. (2013) Magnesium isotope evidence for single stage formation of CB chondrules by colliding planetesimals. *Astrophys. J.* **776**, L1–L6.

Oulton J., Humayun M., Fedkin A. and Grossman L. (2015) Chemical evidence from Gujba for differentiation and evaporation/re-condensation processes during the CB-impact event. *Lunar Planet. Sci. Conf.* **46**. Abstract#1590.

Prombo C. A. and Clayton R. N. (1985) A striking nitrogen isotope anomaly in the Bencubbin and Weatherford meteorites. *Science* **230**, 935–937.

Rubin A. E., Kallemeyn G. W., Wasson J. T., Clayton R. N., Mayeda T. K., Grady M., Verchovsky A. B., Eugster O. and Lorenzetti S. (2003) Formation of metal and silicate globules in Gujba: a new bencubbinite-like meteorite fall. *Geochim. Cosmochim. Acta* **67**, 3283–3298.

Ruzicka A. (2012) Chondrule formation by repeated evaporative melting and condensation in collisional debris clouds around planetesimals. *Meteorit. Planet. Sci.* **47**, 2218–2236.

Sanders I. S. (1996) A chondrule-forming scenario involving molten planetesimals. In *Chondrules and the Protoplanetary Disk* (eds. R. H. Hewins, R. H. Jones and E. R. D. Scott). Cambridge University Press, Cambridge, pp. 327–334.

Sanders I. S. and Scott E. R. D. (2012) The origin of chondrules and chondrites: debris from low-velocity impacts between molten planetesimals. *Meteorit. Planet. Sci.* **47**, 2170–2192.

Simon S. B. and Grossman L. (2004) A preferred method for the determination of bulk compositions of coarse-grained refractory inclusions and some implications of the results. *Geochim. Cosmochim. Acta* **68**, 4237–4248.

Sugiura N., Zashu S., Weisberg M. and Prinz M. (2000) A nitrogen isotope study of bencubbinites. *Meteorit. Planet. Sci.* **36**, 987–996.

Taylor S. R. and McLennan S. M. (2009) *Planetary Crusts: Their Composition*. Cambridge University Press, Cambridge, UK, Origin and Evolution, pp. 378.

Taylor G. J., Scott E. R. D. and Keil K. (1983) Cosmic setting for chondrule formation. In *Chondrules and Their Origins* (ed. E. A. King). Lunar & Planetary Institute, Houston, Texas, pp. 262–278.

van Niekirk D., Humayun M. and Keil K. (2009) In situ determination of siderophile trace elements in EL3 meteorites. *LPSC* **XL**, abstracts (#2049), LPI, Houston (CD-ROM).

Wang J., Davis A. M., Clayton R. N., Mayeda T. K. and Hashimoto A. (2001) Chemical and isotopic fractionation during the evaporation of the FeO–MgO–SiO_2–CaO–Al_2O_3–TiO_2 rare earth element melt system. *Geochim. Cosmochim. Acta* **65**, 479–494.

Wasson J. T. and Kallemeyn G. W. (1990) Allan Hills 85085: a subchondritic meteorite of mixed nebular and regolithic heritage. *Earth Planet. Sci. Lett.* **101**, 148–161.

Weisberg M. K. and Kimura M. (2010) Petrology and Raman microscopy of high pressure phases in the Gujba CB chondrite and the shock history of the CB parent body. *Meteorit. Planet. Sci.* **45**, 873–884.

Weisberg M., Prinz M. and Nehru C. E. (1990) The Bencubbin chondrite breccia and its relationship to CR chondrites and the ALH85085 chondrite. *Meteoritics* **25**, 269–279.

Weisberg M. K., Prinz M., Clayton R. N. and Mayeda T. K. (1993) The CR (Renazzo-type) carbonaceous chondrite group and its implications. *Geochim. Cosmochim. Acta* **57**, 1567–1586.

Weisberg M. K., Prinz M., Clayton R. N., Mayeda T. K., Sugiura N., Zashu S. and Ebihara M. (2001) A new metal-rich chondrite grouplet. *Meteorit. Planet. Sci.* **36**, 401–418.

Yang S., Humayun M., Righter K., Jefferson G., Fields D. and Irving A. J. (2015) Siderophile and chalcophile element abundances in shergottites: implications for Martian core formation. *Meteorit. Planet. Sci.* **50**, 691–714.

Zanda B. (2004) Chondrules. *Earth Planet. Sci. Lett.* **224**, 1–17.

Zanda B., Bourot-Denise M., Hewins R. H., Cohen B. A., Delaney J. S., Humayun M. and Campbell A. J. (2002) Accretion textures, iron evaporation and re-condensation in Renazzo chondrules. *Lunar Planet. Sci. XXXIII*. Abstract#1852.

Zook H. A. (1981) On a new model for the generation of chondrites. *Lunar. Planet. Sci.* **XII**, 1242–1244.

Associate editor: Alexander N. Krot